Recent developments of PET technique and its applications

Alberto Del Guerra

Functional Imaging and Instrumentation Group
Department of Physics "E. Fermi"
University of Pisa and INFN, Pisa, Italy

http://www.df.unipi.it/~fiig/
Email:alberto.delguerra@df.unipi.it

CONTENTS

- A bit of History
- The Physics of PET
- The Technology of PET
- Molecular Imaging
  - Hybrid Systems I (PET-CT)
  - Hybrid Systems II (PET-MR)
- An application in oncology
- A final digression
- Conclusions

A BIT of HISTORY

The Nobel Prize in Physics 1903

"in recognition of the extraordinary services he has rendered by his discovery of spontaneous radioactivity"

"in recognition of the extraordinary services they have rendered by their joint researches on the radiation phenomena discovered by Professor Henri Becquerel"

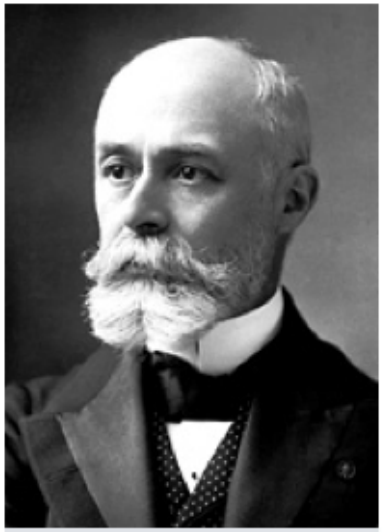

Antoine Henri Becquerel

1/2 of the prize

Pierre Curie

1/4 of the prize

Marie Curie, née Sklodowska

1/4 of the prize

The Nobel Prize in Physics in1936

Discovery of the Positron

August 1932

Carl D. Anderson found evidence for an electron with a positive charge, later called the positron. Anderson discovered the positron while using a cloud chamber to investigate cosmic rays.

C. D. Anderson

1936 Nobel Laureate in Physics

"for his discovery of the positron".

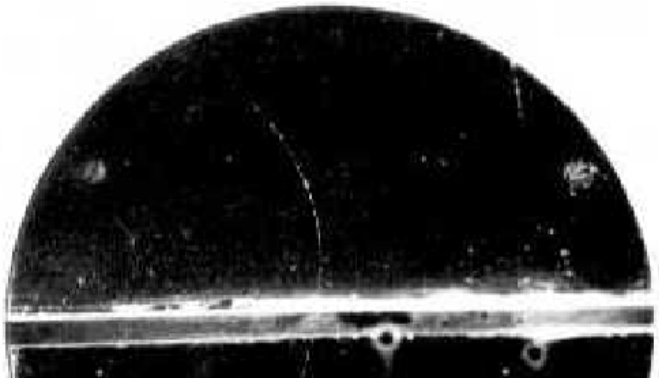

Anderson's first picture of a positron track

The positron travelled downwards and lost energy as it passed through a lead plate in the middle of the chamber. Its track is curved because there was a magnetic field in the chamber

Anderson, C.D.; "*The Apparent Existence of Easily Deflectable Positives*" Science **76** (1932) 238;

Physics

The Nobel Prize in Physics 1939

"for the invention and development of the cyclotron and for results obtained with it, especially with regard to artificial radioactive elements"

Ernest Orlando Lawrence

USA

The Nobel Prize in Chemistry in1943

NUCLEAR MEDICINE

1924: Principle of radiotracer applications:

Changing an atom in a molecule for its radioisotope will not change its chemical and biological behaviour significantly.

Consequence: the movement, distribution, concentration of the molecule can be measured with radiation detectors.

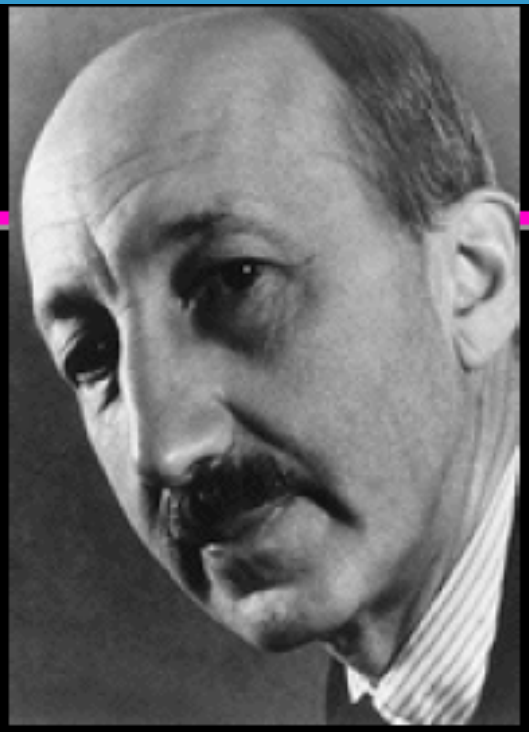

György HEVESY (1885–1966)

1943 Nobel Laureate in Chemistry

„for his work on the use of isotopes as tracers in the study of chemical processes"

50's - The beginning of PET / 1

First Clinical Positron Imaging Device

1952 - This instrument followed the general concepts of the instrument build in 1950 but included many refinements. It produced both a coincidence scan as well as an unbalance scan. The unbalance of the two detectors was used to create an unbalance image using two symbols to record any unbalance in the single channel rates of the two detectors.

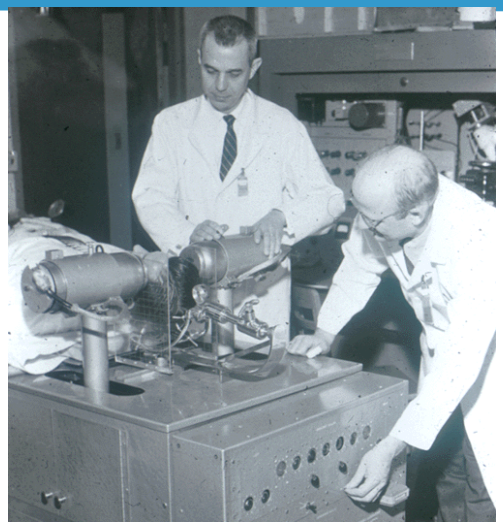

Dr. Brownell (left) and Dr.Aronow are shown with the scanner (1953).

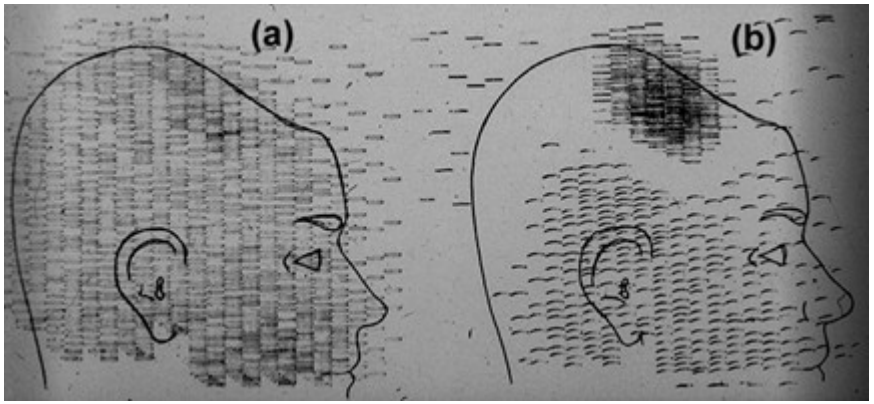

Coincidence and unbalance scans of patient with recurring brain tumor. Coincidence scan (a) of a patient showing recurrence of tumor under previous operation site, and unbalance scan (b) showing asymmetry to the left. (Reproduced from Brownell and Sweet 1953).

70's -The beginning of PET/2

Positron emission tomography

Early '70-s: PET

Principle: Two 511 keV photons resulting from annihilation fly in opposite directions. Their coincident detection determines the line of annihilation

M. E. Phelps

E.J. Hoffman

- Michel M. Ter-Pogossian, Mallinckrodt Institute
- Michael E. Phelps, UCLA
- Edward J. Hoffman, UCLA

The PHYSICS of PET

The radioactive decay

- **Isotope decays, emitting β^+.**

  ^{18}F 2 hour half-life

  ^{15}O, ^{11}C, ^{13}N 2–20 minute half-life

- **β^+ annihilates with e^- from tissue, forming back-to-back 511 keV photon pair.**
- **511 keV photon pairs detected via time coincidence.**
- **Positron lies on line defined by detector pair (Line of FLIGHT =LOF ➔ LOR).**

The annihilation process

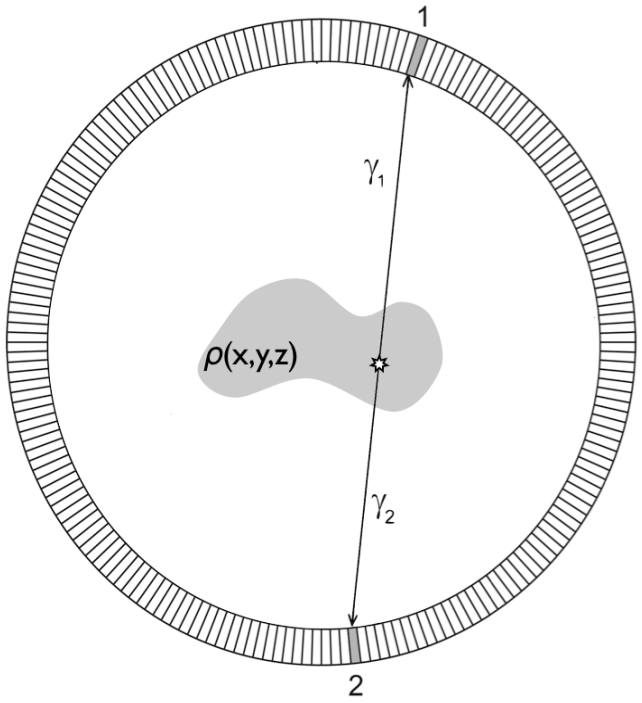

The collinear emission of an annihilation γ-ray pair defines the Line-Of-Flight (LOF). The LOFs are collected by surrounding the object with a "ring" of detectors.

The activity distribution ρ(x,y,z) is measured in terms of projections ($N_{\gamma\text{-}\gamma}$) along lines L.

Each projection is obtained from the activity distribution with the line integral operator:

$$N_{\gamma-\gamma} = k \int_L \rho(x, y, z)\, dl$$

The block detector (*)

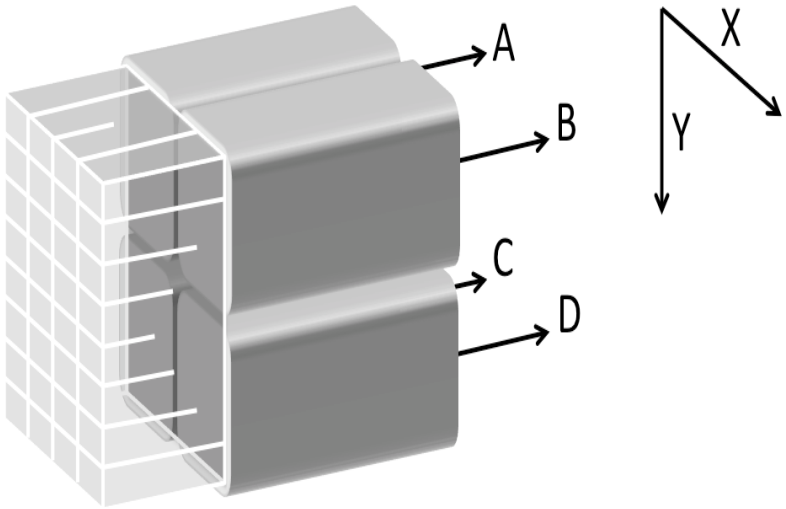

Scheme of a Block Detector.

A block of scintillator is subdivided by cuts at different depths into 4×8 rectangular elements.

The block is read out by a matrix of 2×2 photomultiplier tubes (outputs S_A, S_B, S_C and S_D).

(*) Casey M.E., Nutt R. *IEEE Trans. Nucl. Sci.* 33, n° 1 (1986): 460-463.

Properties of the Scintillators (*)

	NaI	BGO	GSO	LSO	LYSO	LGSO	LuAP	YAP	$LaBr_3$
Light yield 10^3 ph/MeV	38	9	8	30	32	16	12	17	60
Primary decay time	250	300	60	40	41	65	18	30	16
ΔE/E (%) at 662 keV	6	10	8	10	10	9	15	4.4	3
Density (g/cm^3)	3.67	7.13	6.71	7.35	7.19	6.5	8.34	5.5	5.08
Effective Z_{eff}	50	73	58	65	64	59	65	33	46
1/μ @ 511 keV (mm)	25.9	11.2	15.0	12.3	12.6	14.3	11.0	21.3	22.3
PE (%) at 511 keV	18	44	26	34	33	28	32	4.4	14

(*) Adapted from Lecomte R. *Eur J Nucl Med Mol Imaging* 36, n° Suppl. 1 (2009): S69–S85.

The TECHNOLOGY of PET

Spatial Resolution

$$FWHM = 1.2\sqrt{\left(\frac{d}{2}\right)^2 + b^2 + (0.0022D)^2 + r^2 + p^2}$$

1.2	**from analytical algorithm (FBP)**
d/2	**from the detector pitch**
b	**from the coding**
0.0022D	**from the 2 photon a-collinearity**
r	**from the positron range**
p	**from parallax**

Effect of positron Range, a-collinearity and parallax

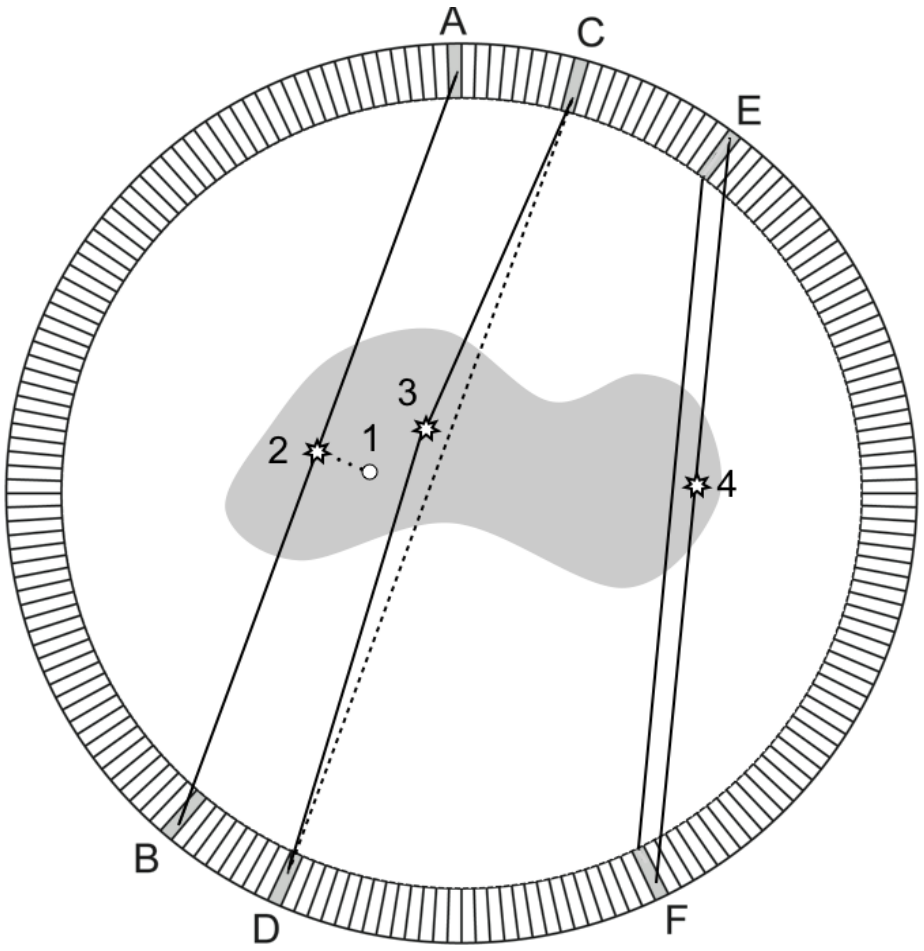

A positron is emitted in 1 and annihilates in 2 due to its finite range. The two annihilation γ-rays are detected in A and B defining a LOR that does not pass by 1.

An annihilation occurs in 3 and two quasi-collinear γ-rays are detected in C and D. Due to the a-collinearity the defined LOR does not pass by 3.

An annihilation occurs at the borders of the FOV in 4 and the two γ-rays are detected in E and F. Due to the uncertainty in the measure of the depth of interaction a parallax error occurs and the LOR defined by the two detectors does not pass from 4.

Positron Range Contribution

Isotope	Average E_k (MeV)	Effective range in water (mm)	FWHM (mm)	FWTM (mm)
^{18}F	0.242	0.54	0.10	1.03
^{11}C	0.385	0.92	0.28	1.86
^{15}O	0.735	2.4	0.50	4.14
^{68}Ga	0.740	2.8	0.58	4.83

Representation of True (T), Scatter (S) and Random (R) events

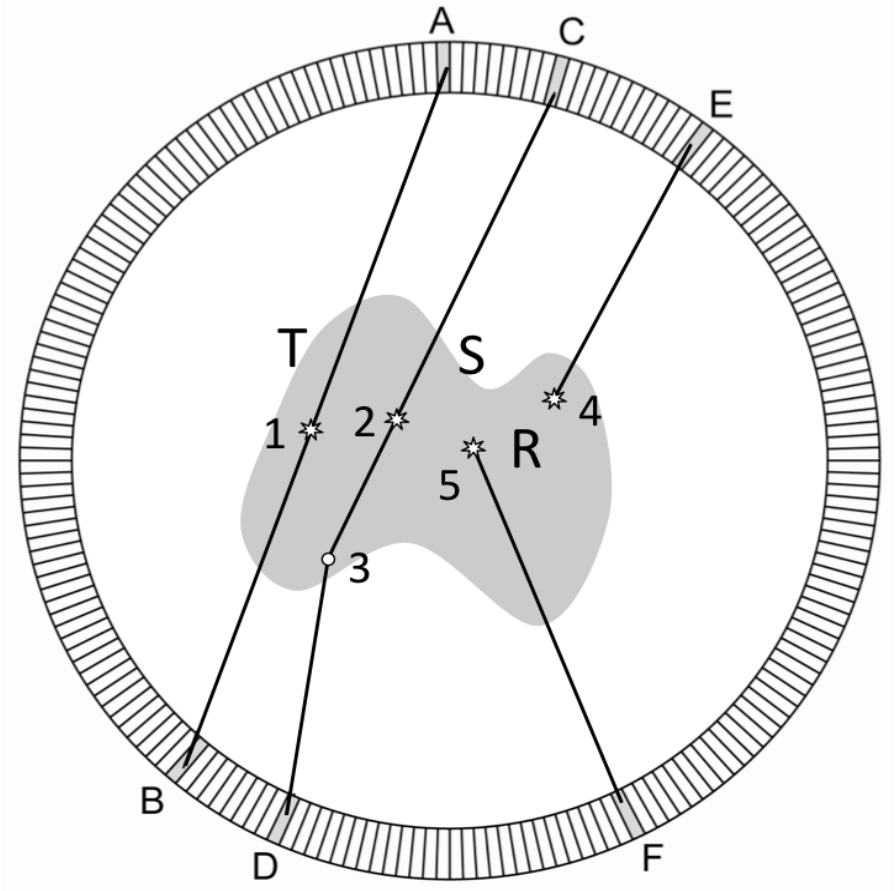

A true coincidence is generated in point 1 and the annihilation photons are detected in opposing crystals A and B.

A Scatter coincidence is generated in point 2 and one annihilation photon is detected in crystal C while the other is detected in opposing crystal D after a Compton scattering interaction in 3.

A random coincidence is detected in opposing crystals E and F for two annihilations in 4 and 5 occurring with a time difference shorter that the coincidence window.

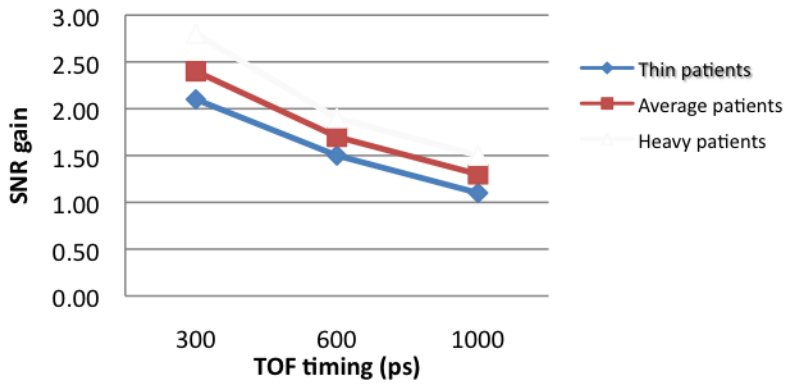
3.00
2.50
2.00
1.50
1.00
0.50
0.00
SNR gain
300
600
1000
TOF timing (ps)
Thin patients
Average patients
Heavy patients

Where the excess noise factor (ENF) describes the statistical noise due to the stochastic multiplication process (Musienko Y. 2008)

Time Resolution

From the Hyman theory (negligible rise time of the scintillation signal)

$$\Delta t \propto \frac{\sqrt{\tau}}{\sqrt{N_{phe}/ENF}}$$

τ: decay time of the fast component

N_{phe}: number of photoelectrons generated by the fast component

ENF: Photodetector excess noise factor

Where the excess noise factor (ENF) describes the statistical noise due to the stochastic multiplication process

NOISE Equivalent Count (Rates) NEC(R)

$$NEC = \frac{T^2}{R_{TOT}}$$

$$R_{TOT} = T + S + kR$$

Where R_{TOT} is the sum of true, random and scatter counts

And k is a factor depending on the method used for measuring the random count rate.

NEC is an indirect measure of the noise in the data due to scatter and random events but also due to the effect of dead time at high count rates.

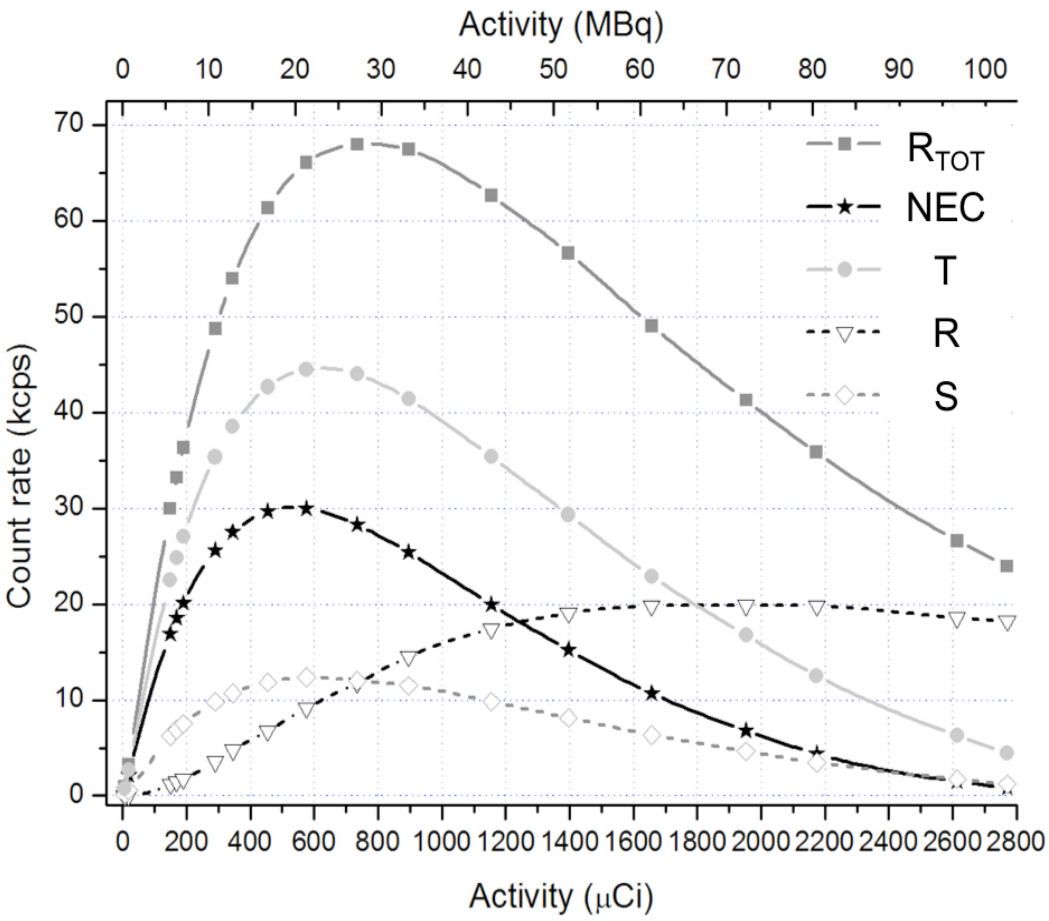

Example of the plot of T, R, S, R_{TOT} and NEC for an animal scanner and a given phantom (custom mouse phantom).

Note the behavior of the NEC curve with the typical peak (30 cps @ 500 μCi in the example).

Increasing Spatial Resolution

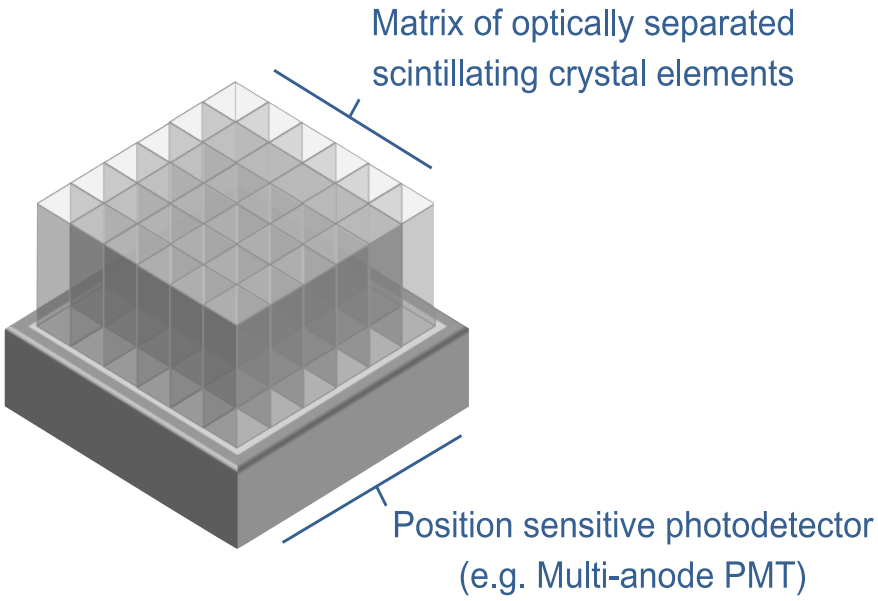

Left: A possible configuration of a PET detector comprised of a MA-PMT and a matrix of scintillating crystals. In this case, the pixel size contribution in the spatial resolution formula is *d*/2 while the coding factor is *b*>0.

Right: The popular Hamamatsu H8500 with 8×8 independent anodes. Its main features are minimum peripheral dead zone (1 mm) and minimal height (12 mm).

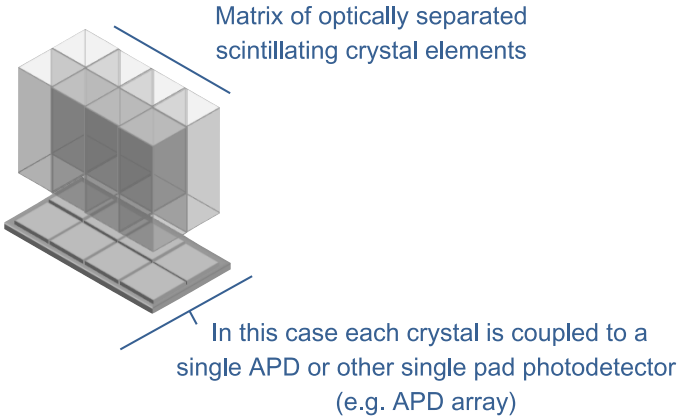

An example of one-to-one coupling using matrices of solid state photodetectors. In this case, the pixel size contribution in the spatial resolution formula is $d/2$ while the coding factor is b=0.

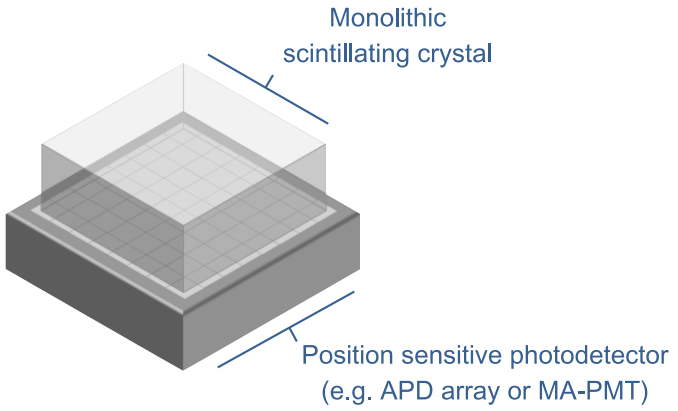

An example of a monolithic scintillating crystal coupled to a position sensitive photodetector. In this case, the pixel size contribution in the spatial resolution formula is not applicable while a positioning factor >0 replaces the coding factor.

(NEW) SOLID STATE PHOTODETECTORS

The Silicon Photomultipliers= SiPM

Silicon PhotoMultiplier = SiPM
Does the dream come true??

SOLID STATE PHOTODETECTOR➔

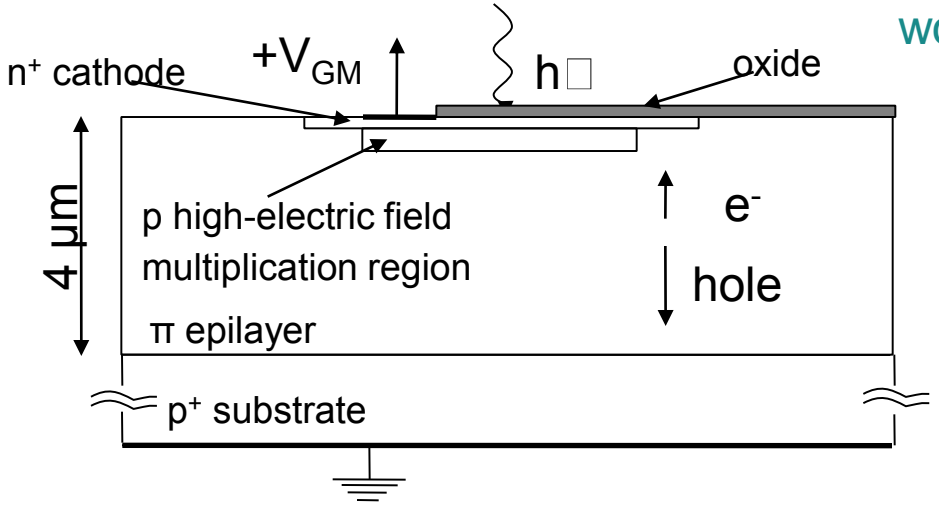

-The photon is absorbed and generates an electron/hole pair

-The electron/hole diffuses or drifts to the high-electric field multiplication region

-The drifted charge undergoes impact ionization and causes an avalanche breakdown.

-Resistor in series to quench the avalanche (limited Geiger mode).

As produced at FBK-irst,Trento, Italy➔

SiPM: **Multicell Avalanche Photodiode** working in limited Geiger mode

- 2D array of microcells: structures in a common bulk.
- Vbias > Vbreakdown: high field in multiplication region
- Microcells work in Geiger mode: the signal is independent of the particle energy
- The SiPM output is the sum of the signals produced in all microcells fired.

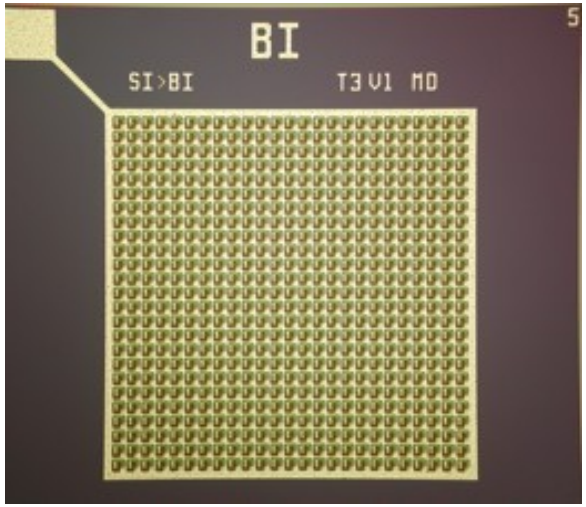

➔High gain ➔Low noise ➔ Good proportionality if $N_{photons} << N_{cells}$

Results: characterization

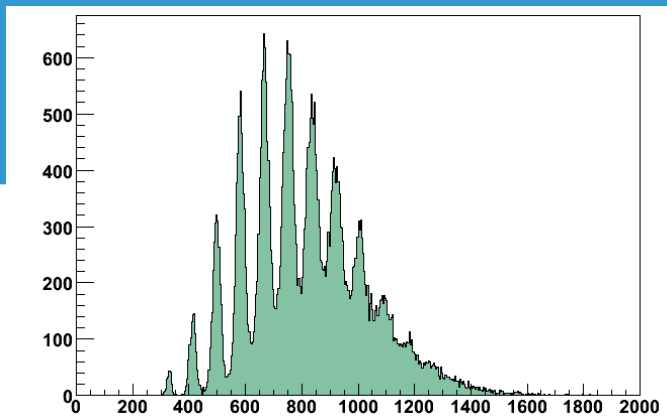

Collaboration with FBK- irst (Trento, Italy), that has been developing SiPMs since 2005:

First detectors - Single SiPMs (2006)

First matrices 2x2 (2007)

First matrices 4x4 (2008)

First matrices 8x8 (2009)

Breakdown voltage V_B ~ 30V**, very good uniformity.**

Single photoelectron **spectrum: well resolved peaks.**

Gain: ~10^6

- Linear for a few volts over V_{BD}.
- Related to the recharge of the diode capacitance C_D from V_{BD} to V_{BIAS} during the avalanche quenching.
  G=(VBIAS-VB) x CD/q

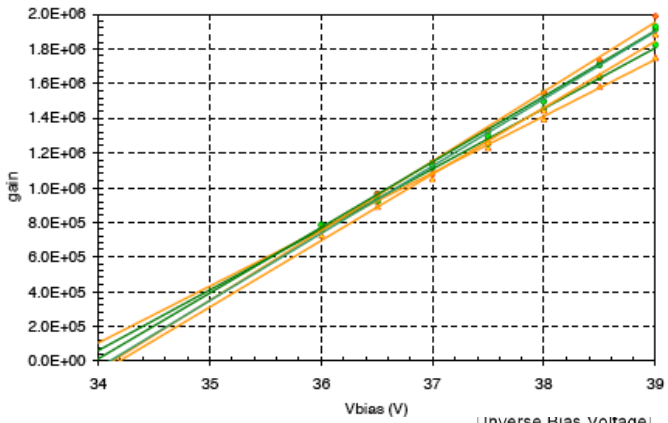

Dark rate:

- 1-3 MHz at 1-2 photoelectron (p.e.) level, ~kHz at 3-4 p.e (room temperature).
- Not a concern for PET applications except for TOFPET

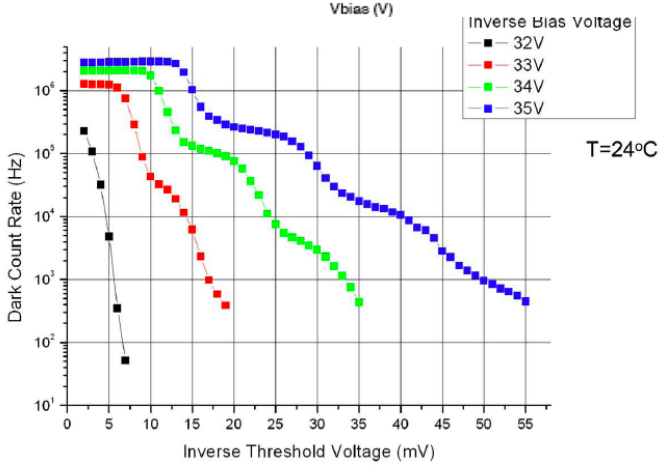

Results: intrinsic timing

Intrinsic timing measured at s.p.e level:
60 ps (σ) for blue light at 4V overvoltage.

SiPM illuminated with a pulsed laser with 60 fs pulse width and 12.34 ns period, with less than 100 fs jitter.

Two wavelengths measured:

λ = 400 ± 7 nm and λ = 800 ± 15 nm.

Time difference between contiguous pulses is determined.

The timing decreases with the number of photoelectrons as

1/√(Npe)➔ 20 ps at 15 photoelectrons.

[G. Collazuol et al., VCI 2007, NIM A 2007, A581, 461-464]

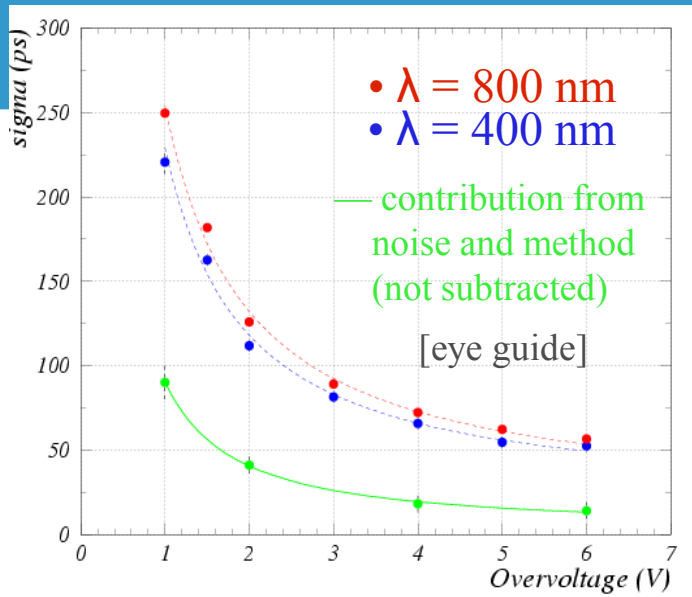

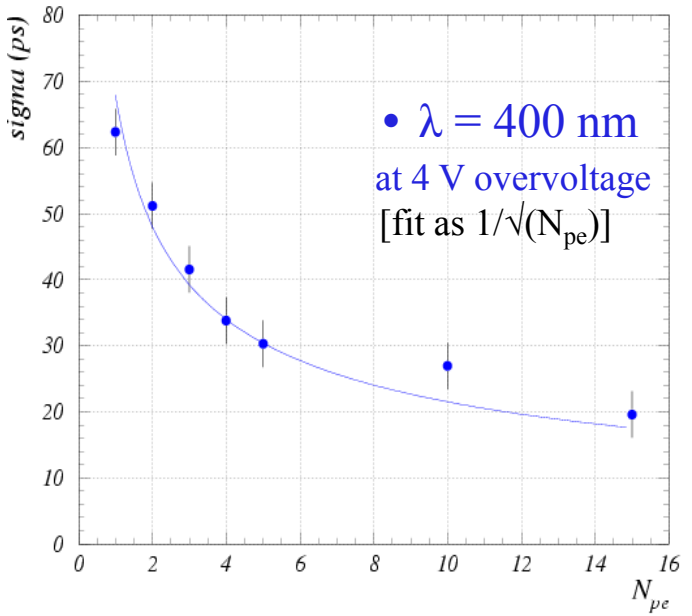

Results: coincidence timing (TOF)

Coincidence measurement with two LSO crystals (1x1x10 mm^3) coupled to two SiPMs {From Theory: **Post and Schiff. Phys. Rev. 80 (1950)1113.**}

$$\sigma \sim \frac{\sqrt{Q}\,\tau}{< N >}$$

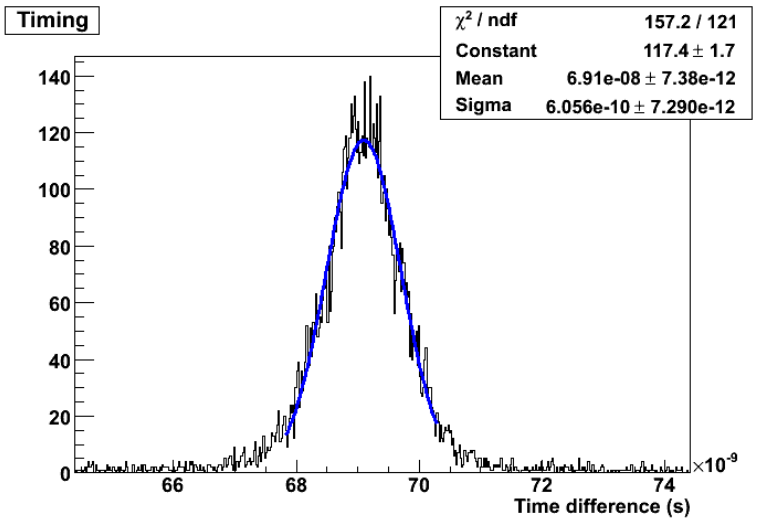

Where:

<N> = average number of photons: ~ 100 photons at the photopeak

Q = Trigger level: ~1 photoelectron.

τ = Decay time of the scintillator

For two scintillators in coincidence expected : => $\sqrt{2}\sigma$~ 630 ps .

Measured => ~ 600 ps sigma.

Measurements in agreement with what we expect!!

[G.Llosa,et al., IEEE Trans. Nucl. Sci. 2008, 55(3), 877-881.

Results: energy resolution (DE/E)

Setup:

- 2 LSO [1mm x 1mm x 10mm] crystals coupled to 2 SiPMs
- Home made amplifier board.
- Time coincidence of signals.
- VME QDC for DAQ.
- ^{22}Na source.

Energy resolution in coincidence: 20% FWHM.
(best result: 17.5 %)

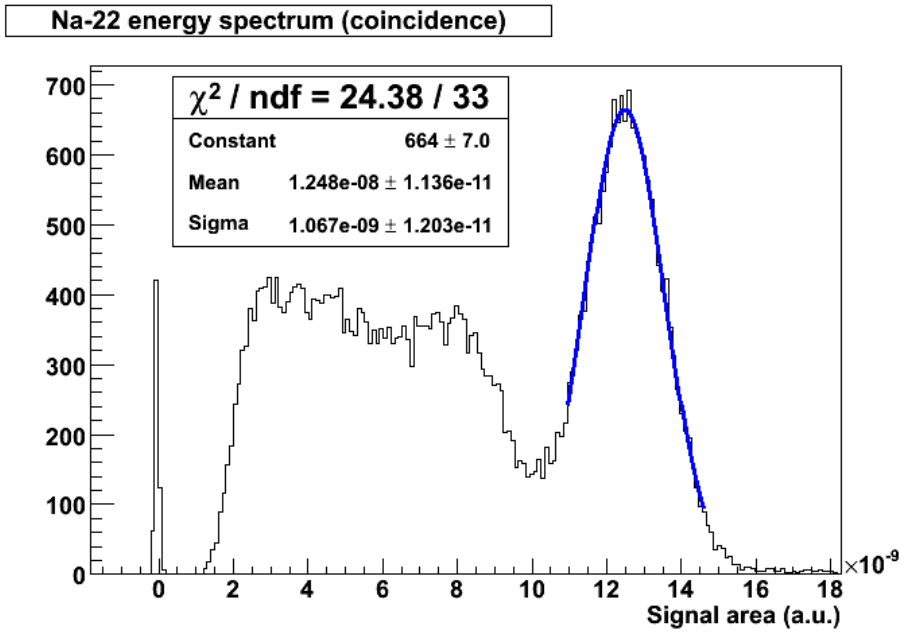

[G.Llosa et al, IEEE Trans. Nucl. Sci. 2008, 55(3), 877-881.]

Results: New detectors (May 2007)

Different geometry,size,microcell size and GF.

40x40μm² => GF 44%
50x50μm² => GF 50%
100x100μm² => GF 76%

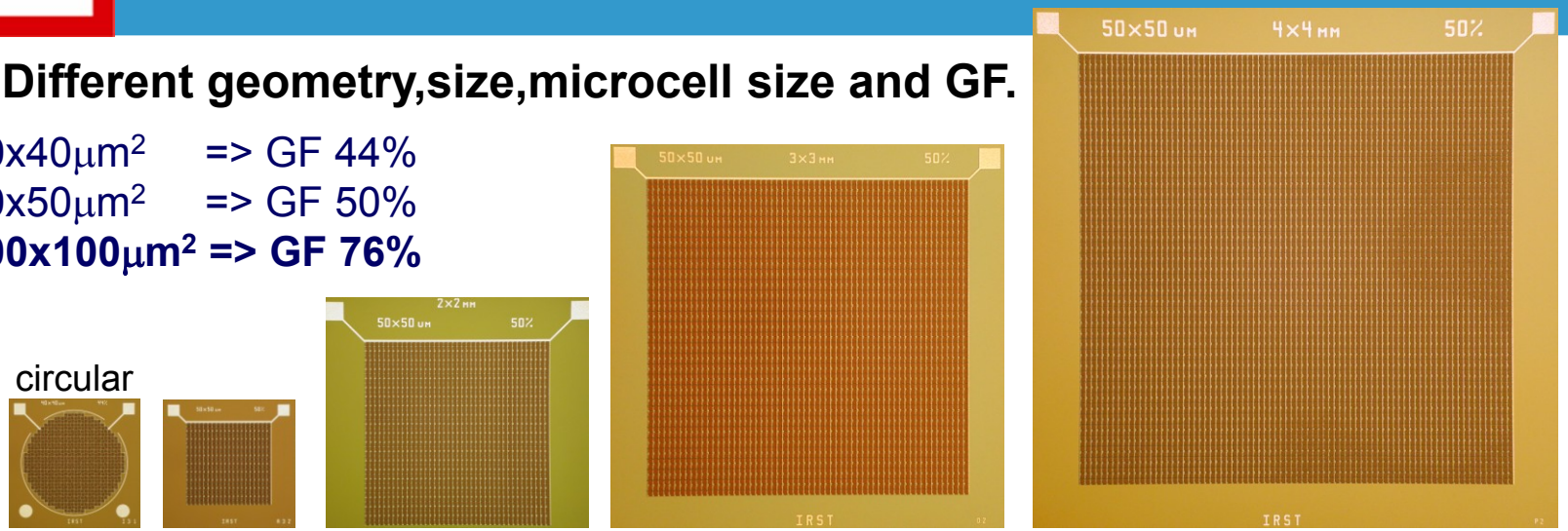

1mm ϕ | 1x1mm² | 2x2mm² | 3x3mm² (3600 cells) | 4x4mm² (6400 cells)

Matrices 16 elements (4x4)

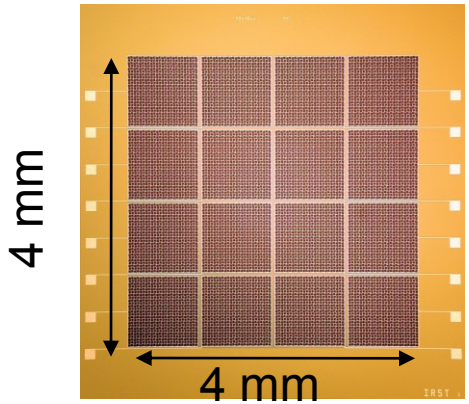

IV CURVES OF 9 MATRICES.

VERY UNIFORM BREAKDOWN POINT

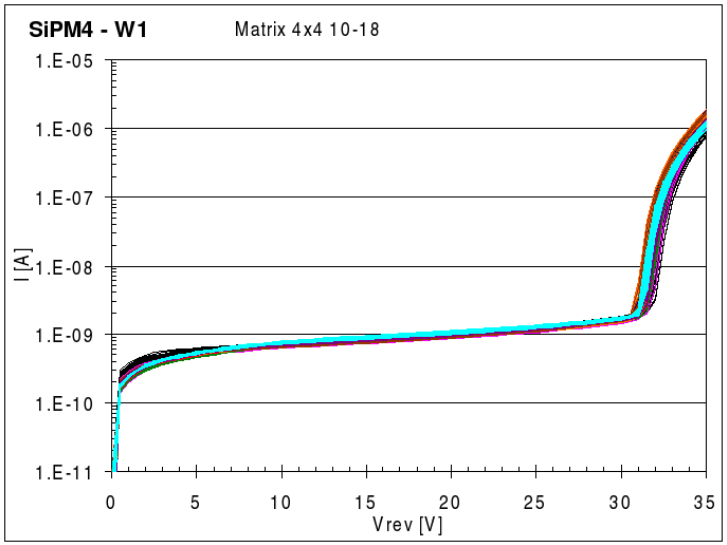

[C.Piemonte et al, Il Nuovo Cimento C, 2007,30(5),473-482]

SiPM 4x4 matrices from FBK-irst

Composed of 16 (4x4) pixel elements in a common substrate
1 mm pixels in 1.06 mm pitch

- Structure: n^+-p-π -p^+ optimized for blue light: Shallow n^+ layer + specific antireflective coating.
- Each pixel: 625 (25 x 25) microcells, 40μm x 40μm size.
- Polysilicon quenching resistor.
- Fill factor 44%.

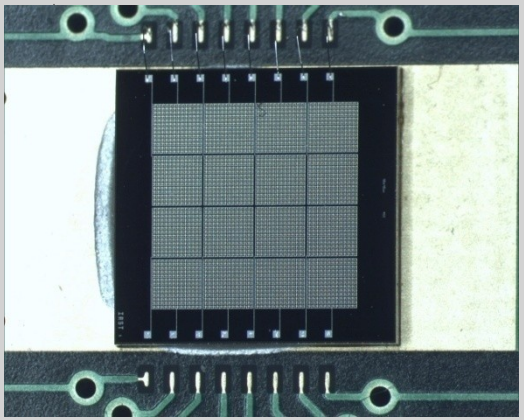

Bonded SiPM array

1 mm

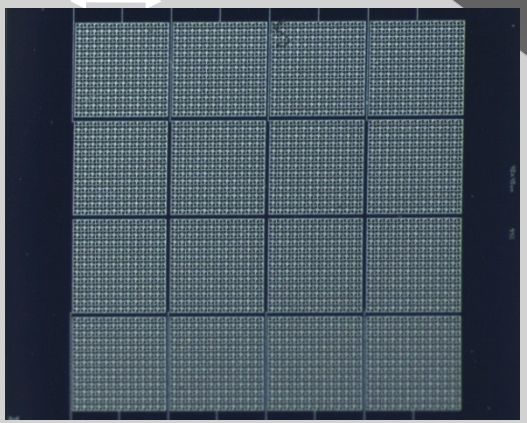

SiPM array

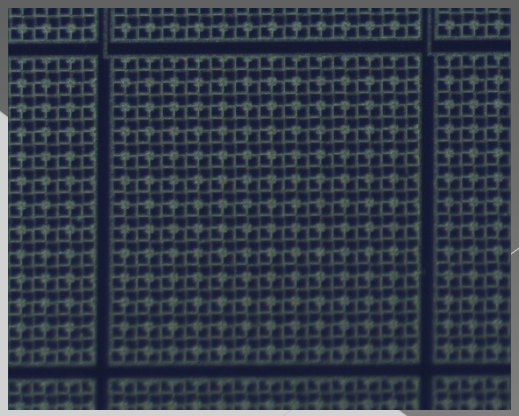

SiPM pixel

Protoytpe DAQ for 2x64 sipm matrices

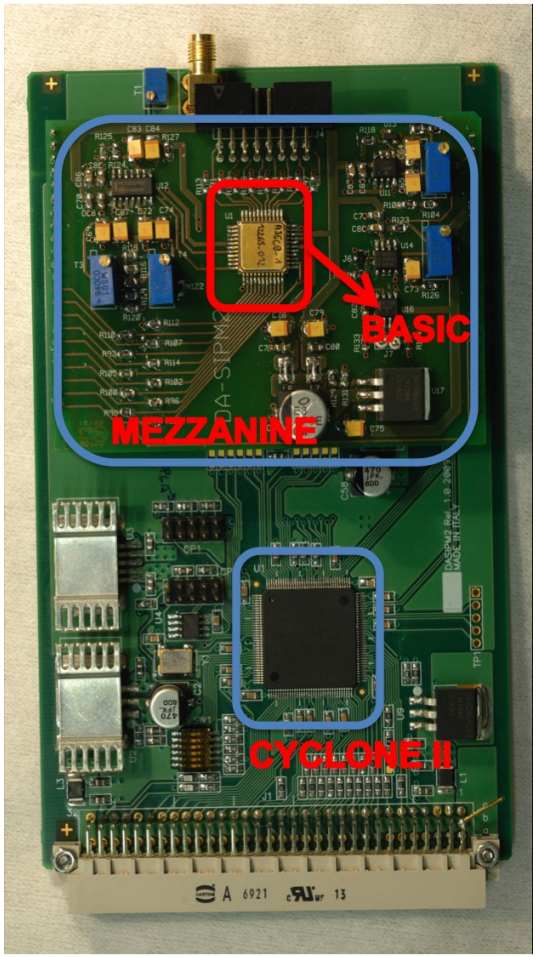

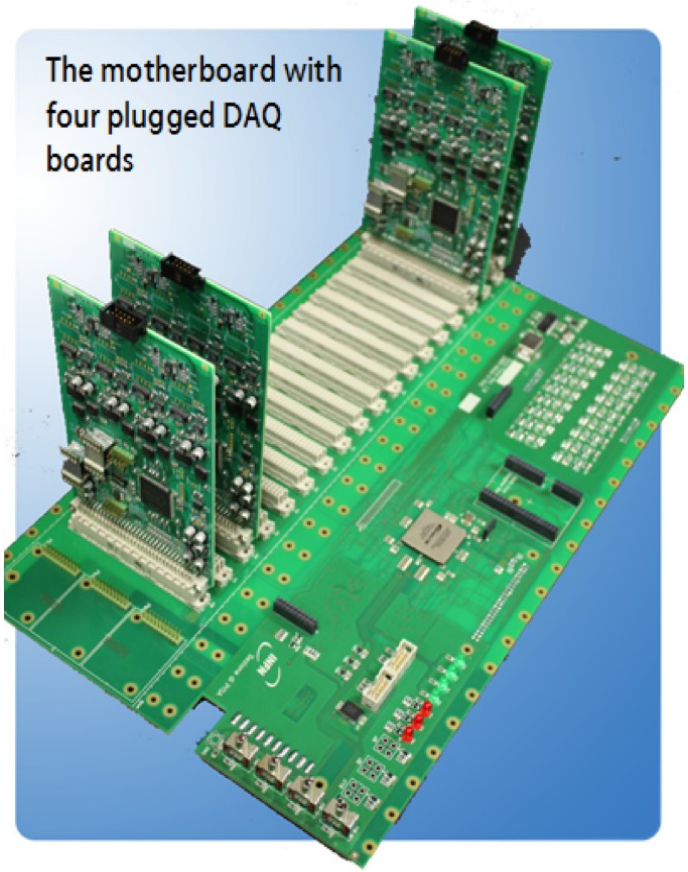

BASIC Timing performance (LSO:Ce,Ca pixel and MPPC)

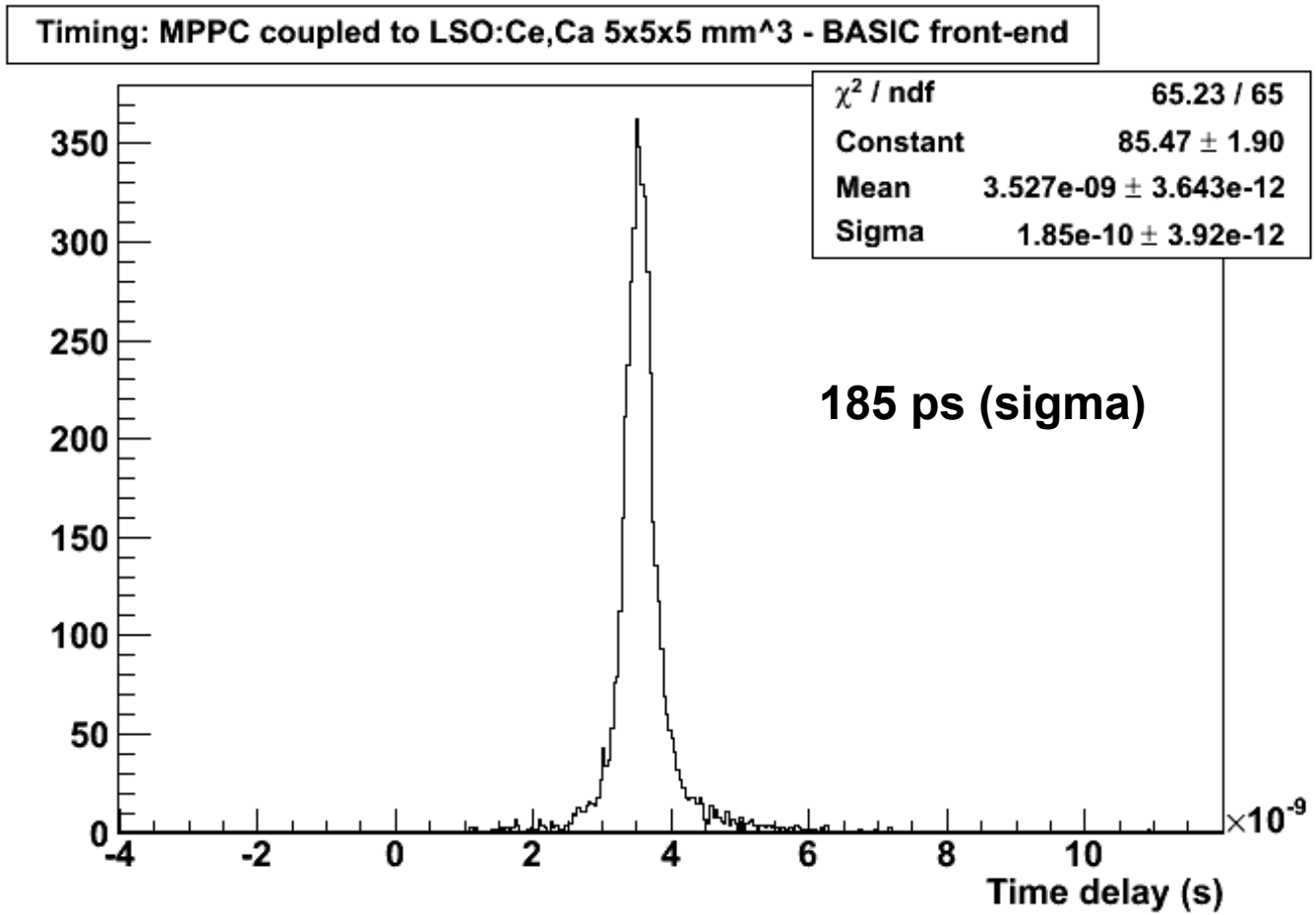

Design concept

- Independent read out from two faces
- Front end ASIC in development
- Cluster processor prototype in FPGA
- Magnetic field compatible design

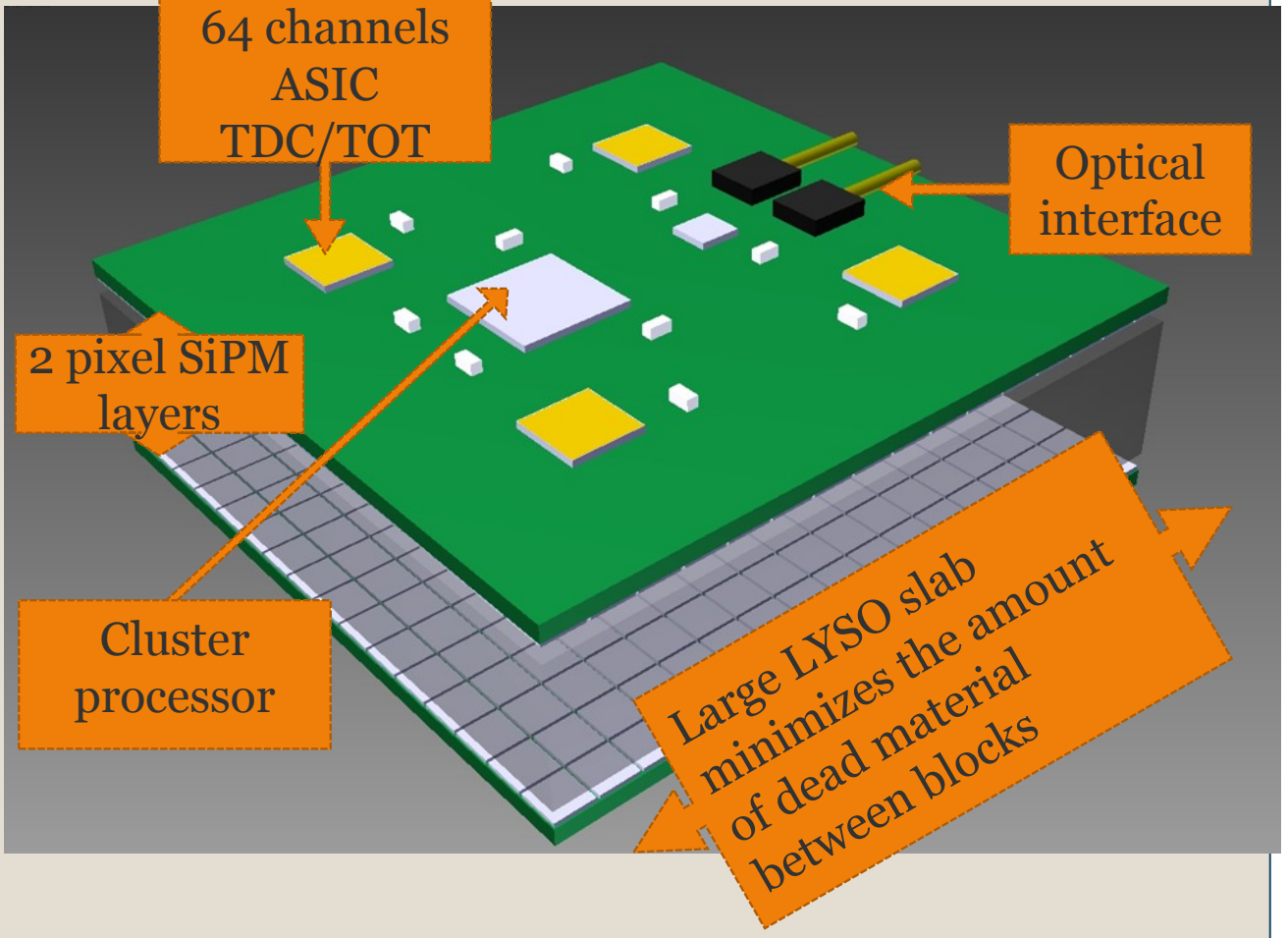

Main features

- Silicon Photomultipliers (SiPM) coupled to a monolitic LYSO scintillator crystal:
  - MRI compatible detectors
  - x and y coordinates determined with high precision
- Time of Flight (TOF):
  - reduces image background noise

$$\frac{S/N_{tof}}{S/N_{non-tof}} = \sqrt{\frac{2D}{c\Delta t}}$$

D = object size

Δt = time resolution

- Depth of Interaction (DOI):
  - decreases the uncertainty of the z coordinate
- Integrated readout electronics for compact time and energy measurement

PMTs vs solid state photodetectors

	PMT	APD	SiPM
Gain	10^5-10^7	10^2	10^5-10^6
Dynamic range	10^6	10^4	10^3/mm
Excess Noise Factor	0.1-0.2	>2	1.1-1.2
Rise time	<1 ns	2-3 ns	~1 ns
Dark current	<0.1 nA/cm^2	1-10 nA/mm^2	0.1-1 MHz/mm^2
QE @ 420 nm	25%[a)]	60-80%	<40%[b)]
Bias voltage	~800-2000 V	~100-1500 V	~30-50 V
Temperature coefficient	<1 %/K	2-3 %/K	3-5 %/K
Magnetic susceptibility	Very high (mT)	No	No

Depth of Interaction = DOI

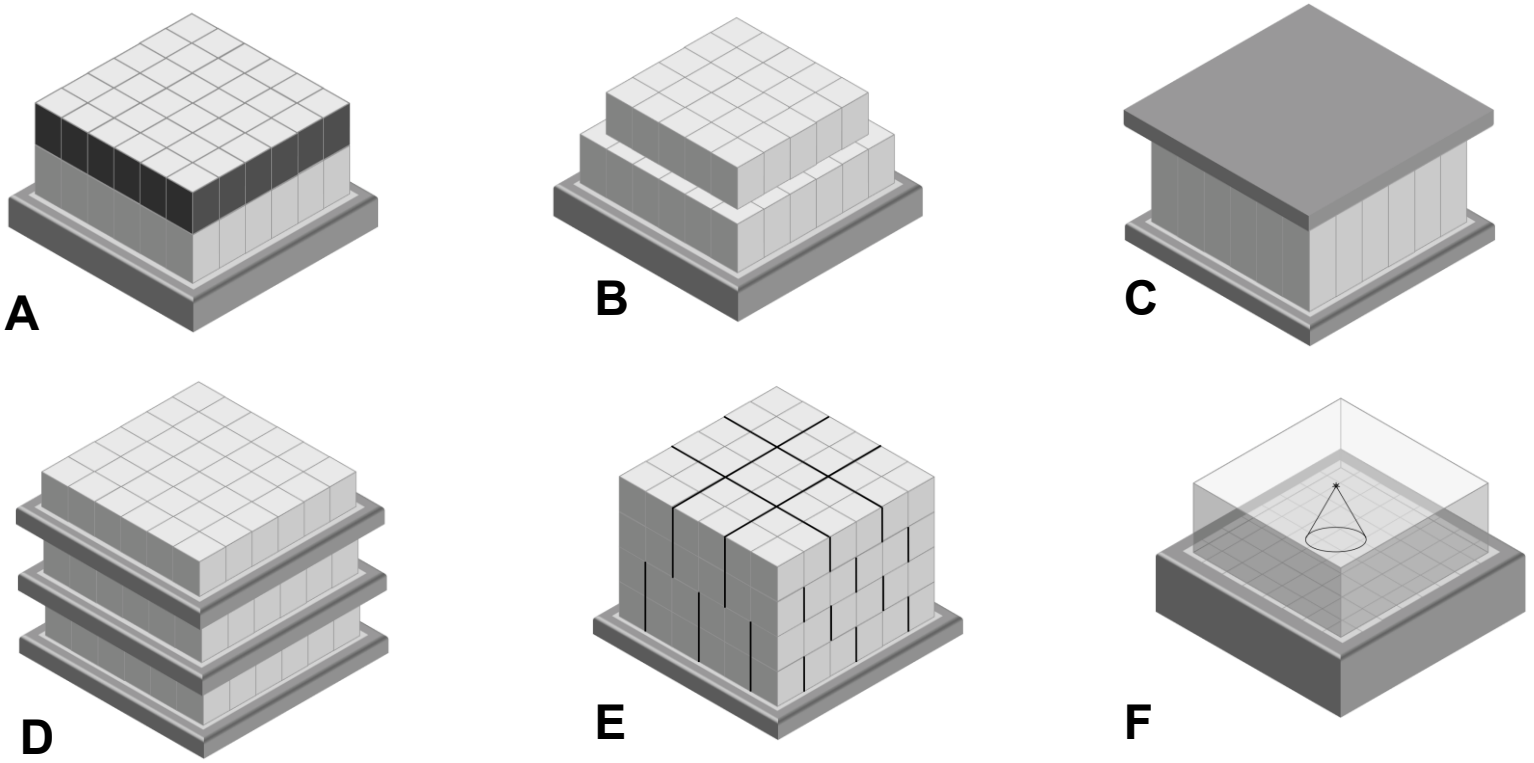

(A)Dual-layer phoswitch (discrete); (B) Dual-layer staggered (C) Dual side readout (continuous); D) Multiple photodetector readout (discrete): E) Multiple layer with reflective pattern (F) Width of the light spot in continuous scintillators (continuous)

PET

➔MEDICAL IMAGING

➔MOLECULAR IMAGING

Molecular Imaging

"A visual representation,characterization, and quantification of biological processes at the cellular and subcellular levels within intact living organisms."

Sanjiv S.Gambhir

CLINICAL SYSTEMS
Hybrid Systems I – PET/CT

Clinical PET applications

Oncology

^{18}F-FDG
Total body

Neurology

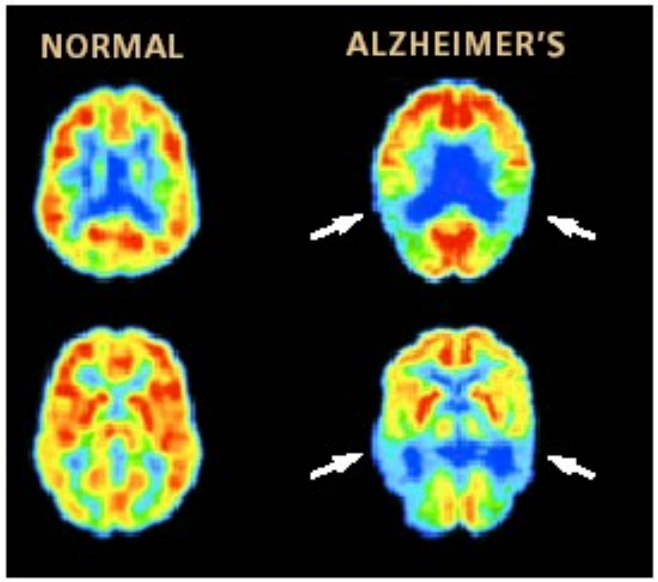

^{18}F-FDG
Brain study for
Alzhemeir's disease

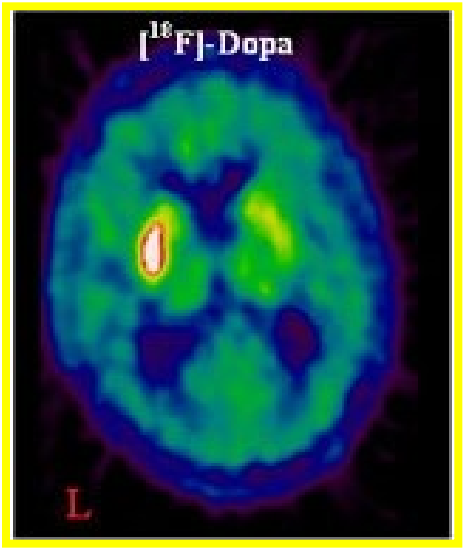

^{18}F-DOPA
Brain study for
Parkinsons's disease

CT technology

- **Spiral CT (With multirow detectors) (> 1998).**

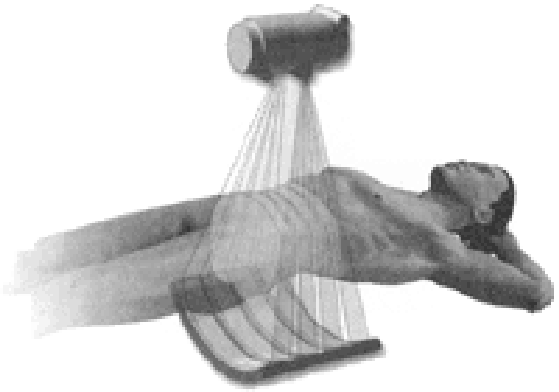

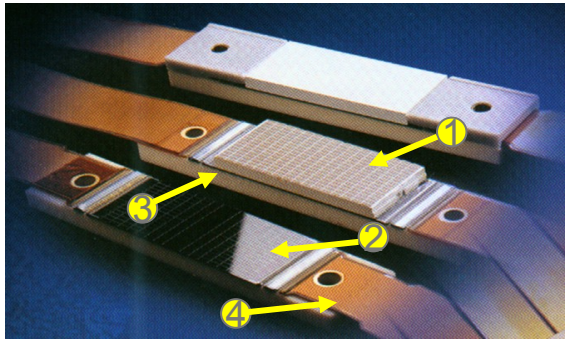

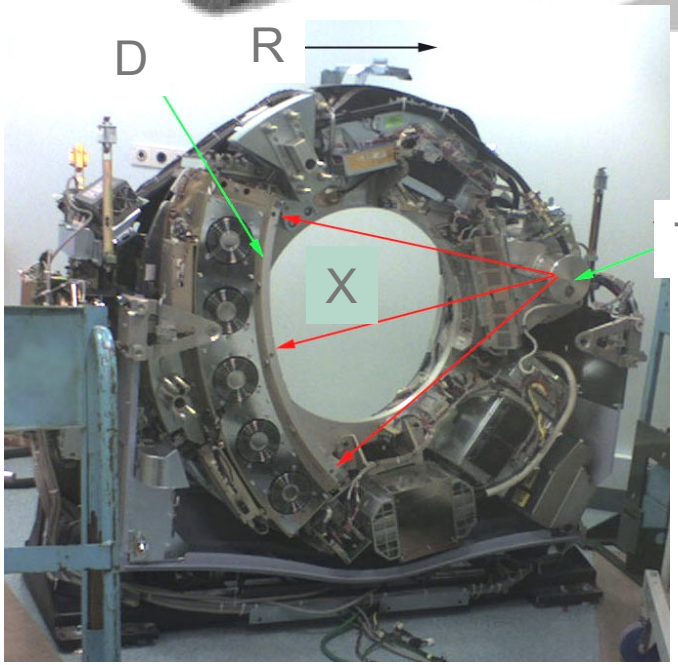

Attenuation correction

- PET needs CT data to anatomically locate the tumor and to correct for the attenuation in order to provide a correct quantification.

- Present systems exploit multislice CT top quality systems, where the number of slices can achieve 128 with rotation time of the order of 300 ms.

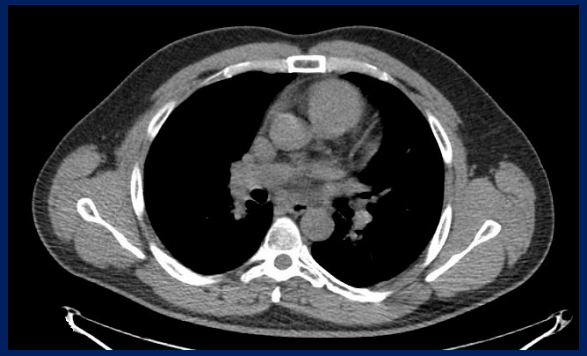

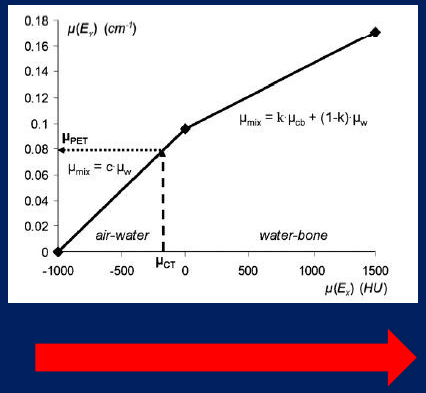

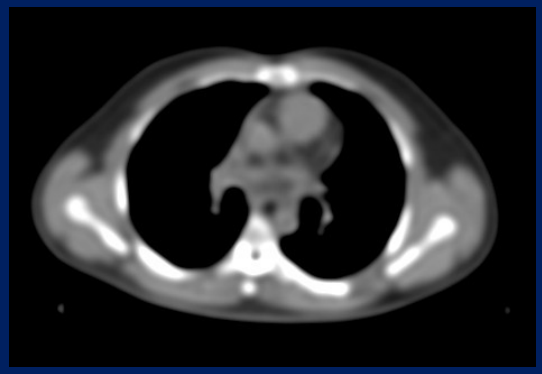

Being the attenuation coefficients (μ) energy dependent, the CT scanning at an average energy of 70 keV must be rescaled (voxel by voxel) to the gamma rays by using a bi-linear scaling function.

Area detector CT – the future of CT

C-Arm CT

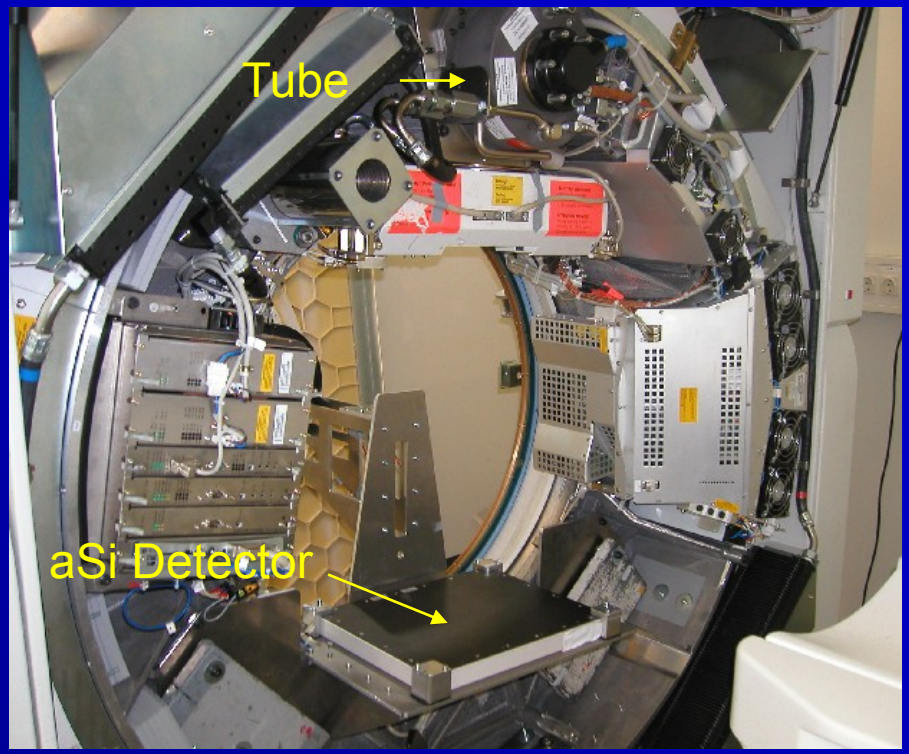

Flat Panel Detector CT

PRECLINICAL SYSTEMS
Hybrid Systems I – PET/CT

“From man to mice” …

Human PET

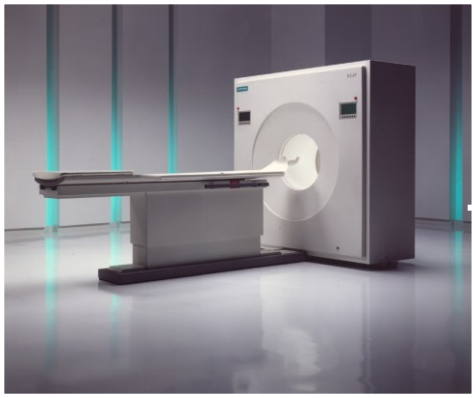

microPET

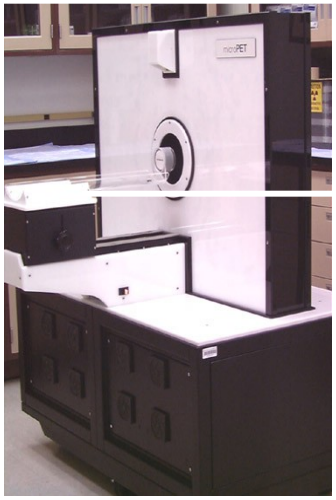

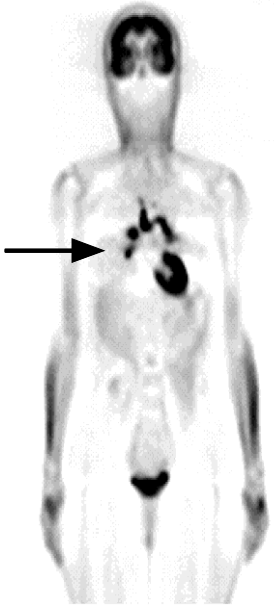

human

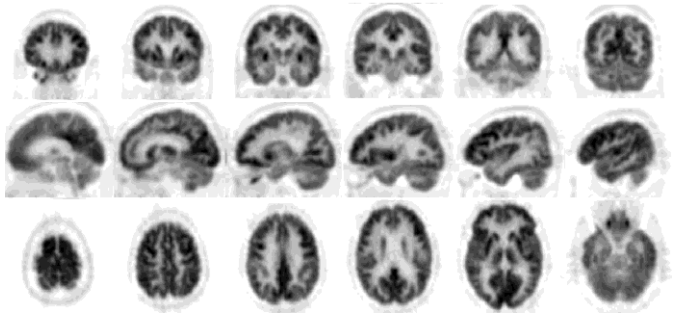

*Images courtesy of Simon Cherry, UCLA

mouse

rat

mouse

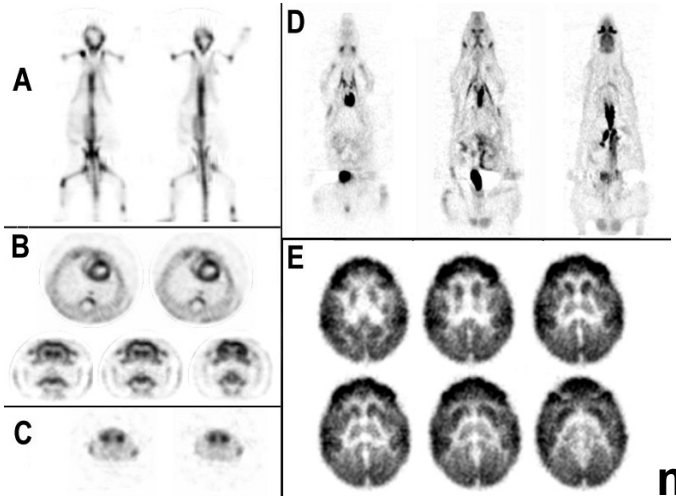

rat

infant monkey

Spatial resolution requirements

Human body: ~70 kg
Heart mass: ~300 g
Aorthic cannula Ø: ~30 mm
Brain cortex apex – temporal lobe: ~105 mm

Rat body: ~200 g
Heart mass: ~1 g
Aorthic cannula Ø: 1.5 - 2.2 mm
Brain cortex apex – temporal lobe: ~10 mm

Mouse body: ~20 g
Heart mass: ~0.1 g
Aorthic cannula Ø: 0.9 - 1.3 mm
Brain cortex apex – temporal lobe: ~6 mm

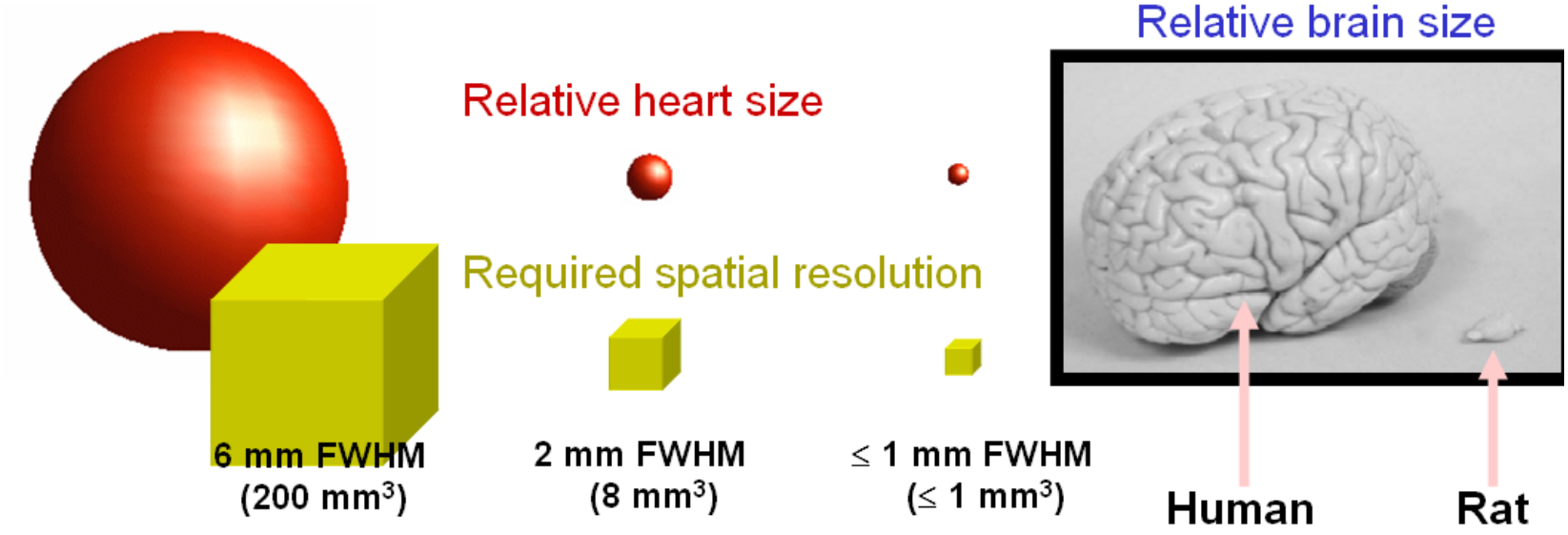

Sensitivity vs Resolution tradeoff

Stationary ring geometry

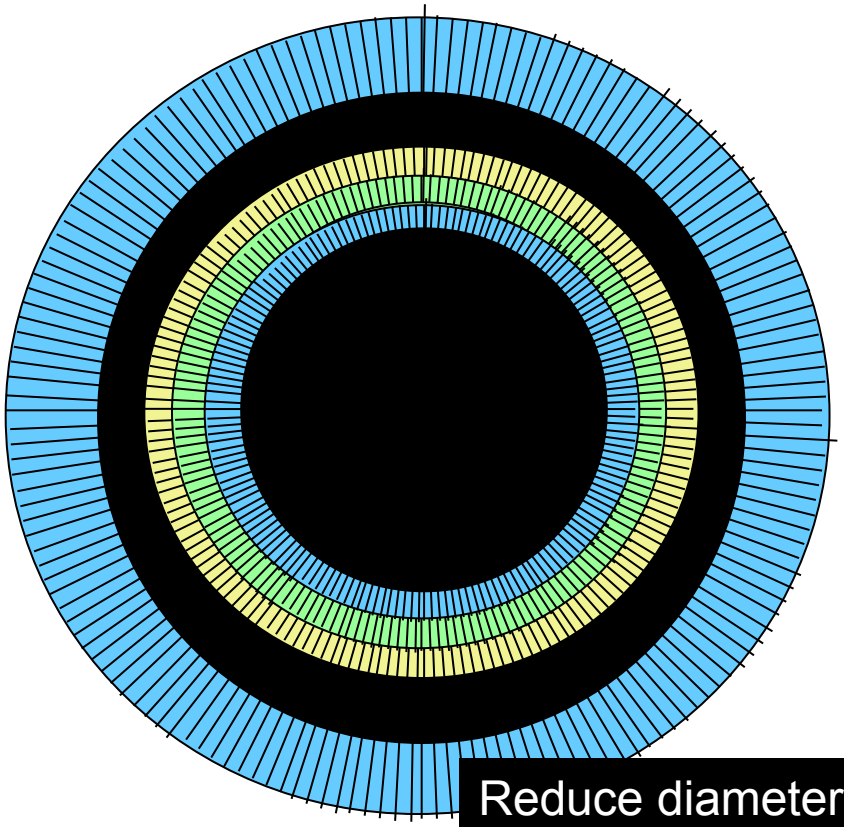

Rotating planar geometry

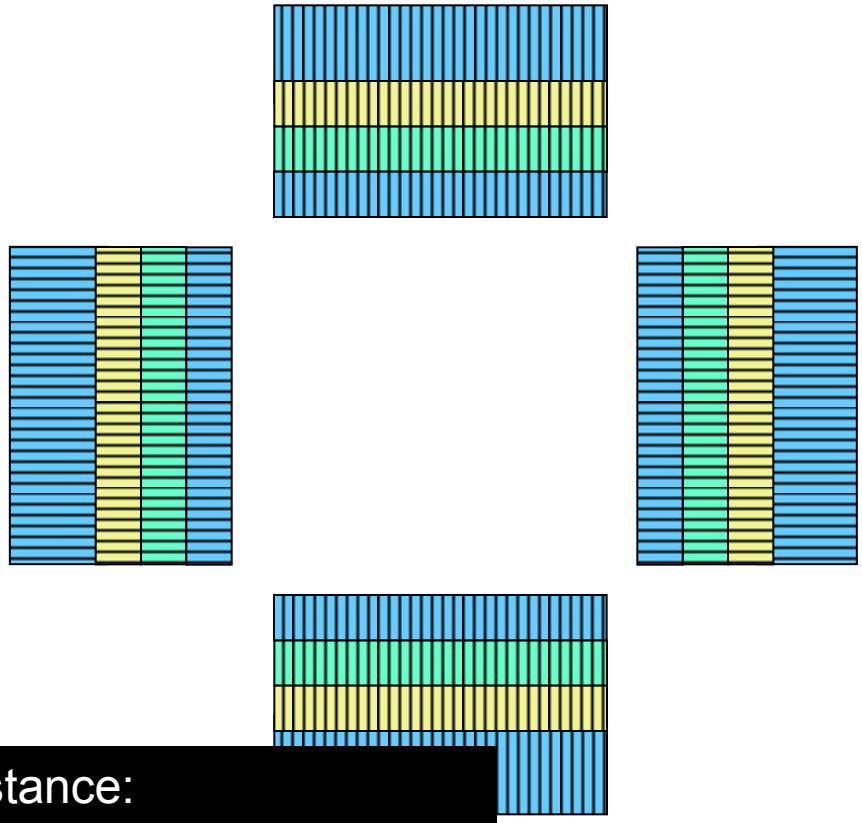

Reduce diameter / distance:
- Increase solid angle coverage
- Less crystals
- Thinner crystals for reducing parallax error

Increase thickness with DOI capability for increasing sensitivity

- Thick scintillator for h… …gh efficiency
- Radial elongation due… …ation due to parallax

YAP-(S)PET II small animal scanner
(originally developed at Ferrara in the early 90's)

yap (s)pet II by FIG

FUNCTIONAL IMAGING AND INSTRUMENTATION GROUP
UNIVERSITY OF PISA

Scanner configuration

Configuration:	**Four rotating heads**
Scintillator:	$YAlO_3$:Ce (YAP:Ce)
Crystal size:	27 x 27 (1.5 x 1.5 x 20 mm^3 each)
Photodetector:	Position Sensitive PMT
Readout method:	Resistive chain (4 channels)
FoV size:	40.5 mm axial × 40.5 mm Ø
Collimators (SPECT):	Lead (parallel holes)
Head-to-head distance:	10-15 cm

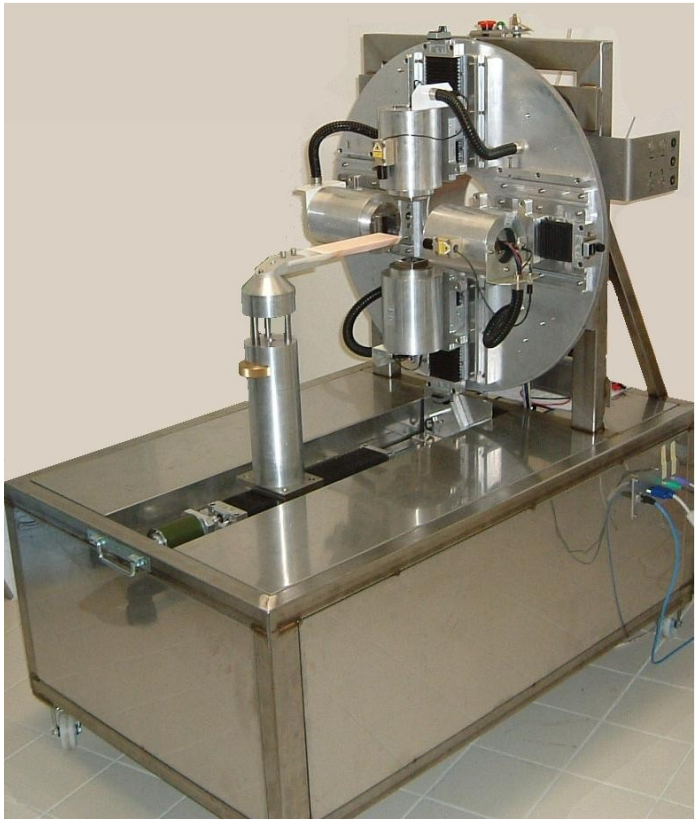

The YAP-(S)PET Scanner is installed at the "Institute of Clinical Physiology" (IFC-CNR) within the framework of the **Center of Excellence AmbiSEN** of the **University of Pisa, Italy**

Heart and bone metabolism in mouse with ^{18}F-FDG and ^{18}F-

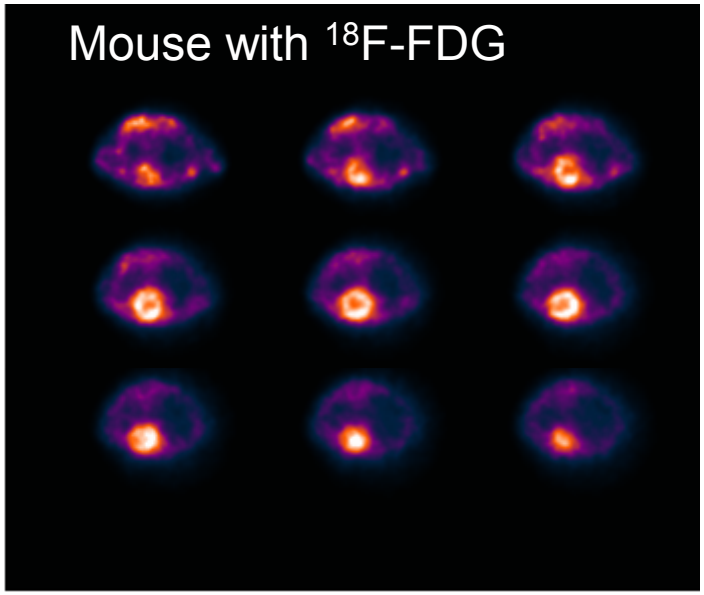

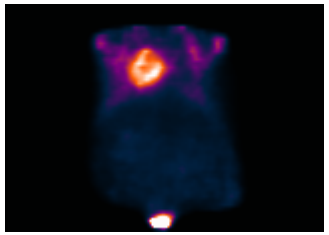

Transaxial sections

Horizontal section

Voxel size:
375 μm × 375 μm × 750 μm
3D ML-EM reconstruction

Mouse with ^{18}F^{-} (post-mortem)

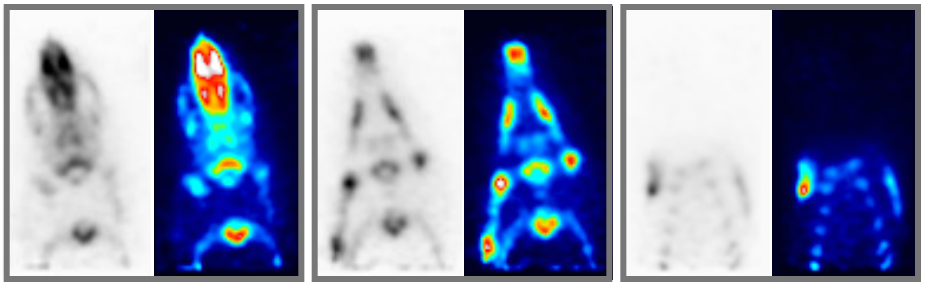

Horizontal slices: Gray and color scale
Injection of 11 MBq of ^{18}F^{-}, uptake time. 120
Step-and-shoot acquisition 128 views/180°
Acquisition time: 60 min

Total body (MIP)
Uptake time:120 min.
Acquisition time:
100 minutes

Small animal CT Xalt$_H$

pixels (48 μm each)
active area
me rate 2.7 fps
olution

Xalt HR

X-ray source

- **Fixed tungsten anode**
- **Maximum voltage: 50 kV**
- **Maximum power: 50 W**
- **Measured focus size: 20 μm FWHM**
- **Beam aperture: 22°**

- **Small animal CT with rotating gantry**
- **Variable geometry (spatial resolution / FOV size trade-off)**
- **Spatial resolution 30 μm**
- **Maximum diameter 8 cm**

Providing in-vivo High resolution image

XaltHR

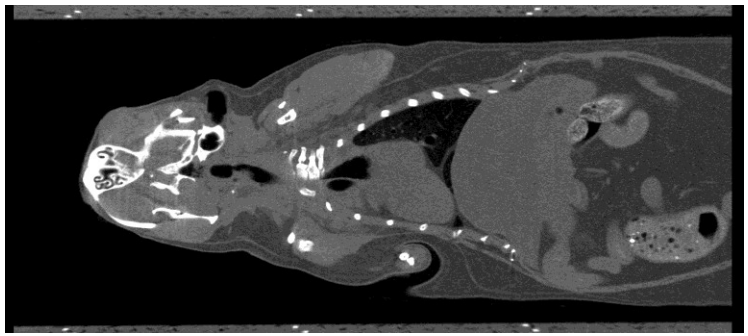

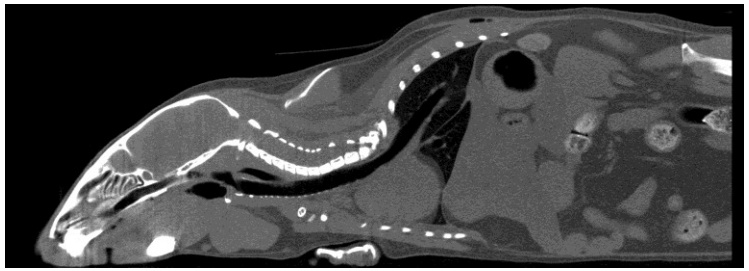

Medical Applications of Micro-CT

Organ / Disease

- **Bone**
- **Teeth**
- **Vessels**
- **Cancer**

Sample / Animal

- **Biopsies**
- **Excised materials**
- **Small animals (rats / mice)**

➔ **in vivo**
ex-vivo
in vitro

Study of stem cells effectiveness for bone regeneration

Scope: Evaluate the efficacy of stem cells in bone regeneration.

Metodology: Right and left femors of rats were treated with a drill injury; only one femor was treated with mesenchimal stem cells (MSC)

MicroCT imaging was performed in-vivo to follow the time evolution of the injury with a resolution of 80 micron. At a certain time point the excised femors were scanned ex-vivo with a resolution of 18 micron.

Assessment of stem cell treatment for bone regeneration

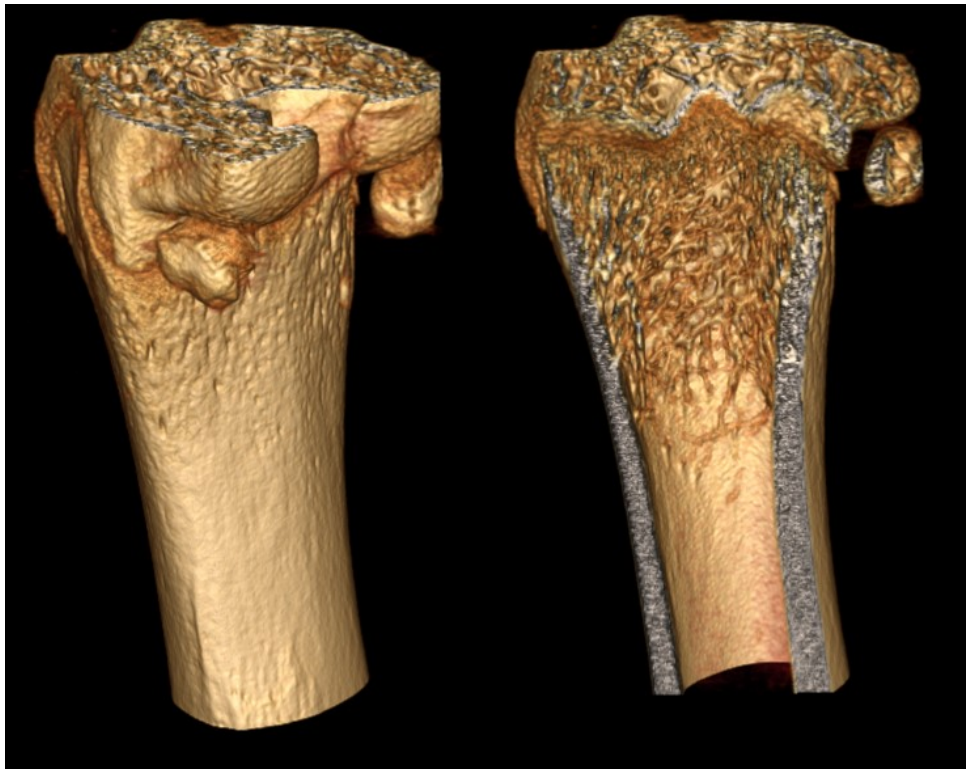

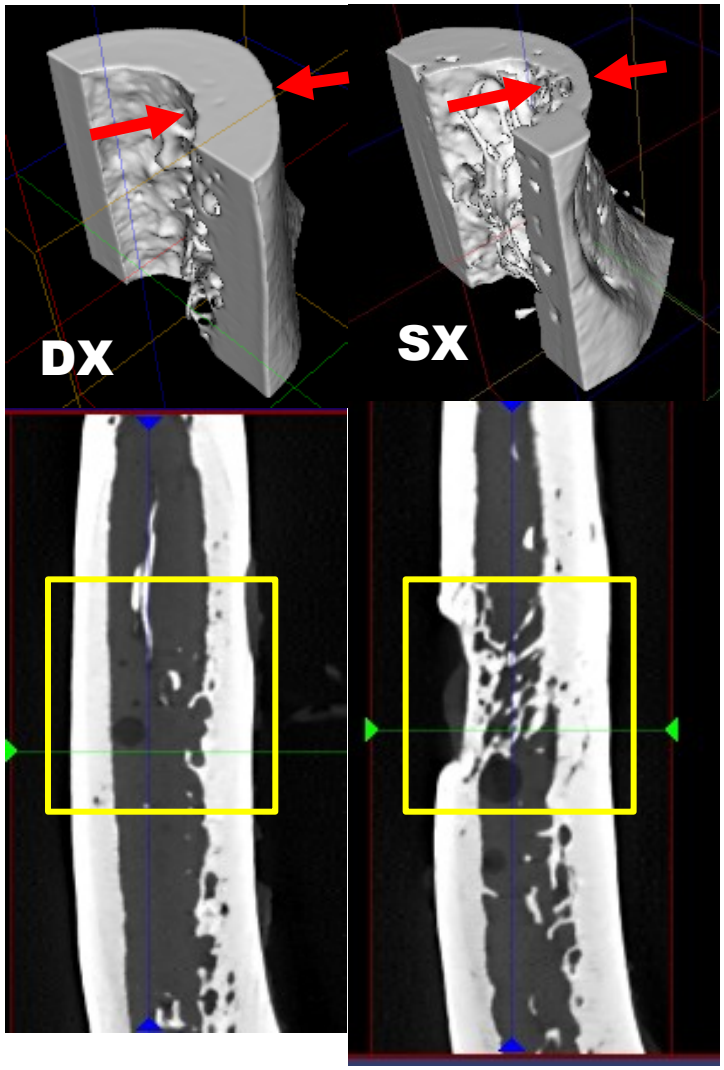

- **High resolution studies on excised femour of rat**

(courtesy of S. Burchielli, FTGM -Pisa
Preliminary and unpublished data, 2010)

Reults: Preliminary images both in vivo and ex vivo seem to show that in the rat femours treated with MSC the speed of repair is faster and the quality of the repaired bone is higher.

YAP-(S)PET + XaltHR

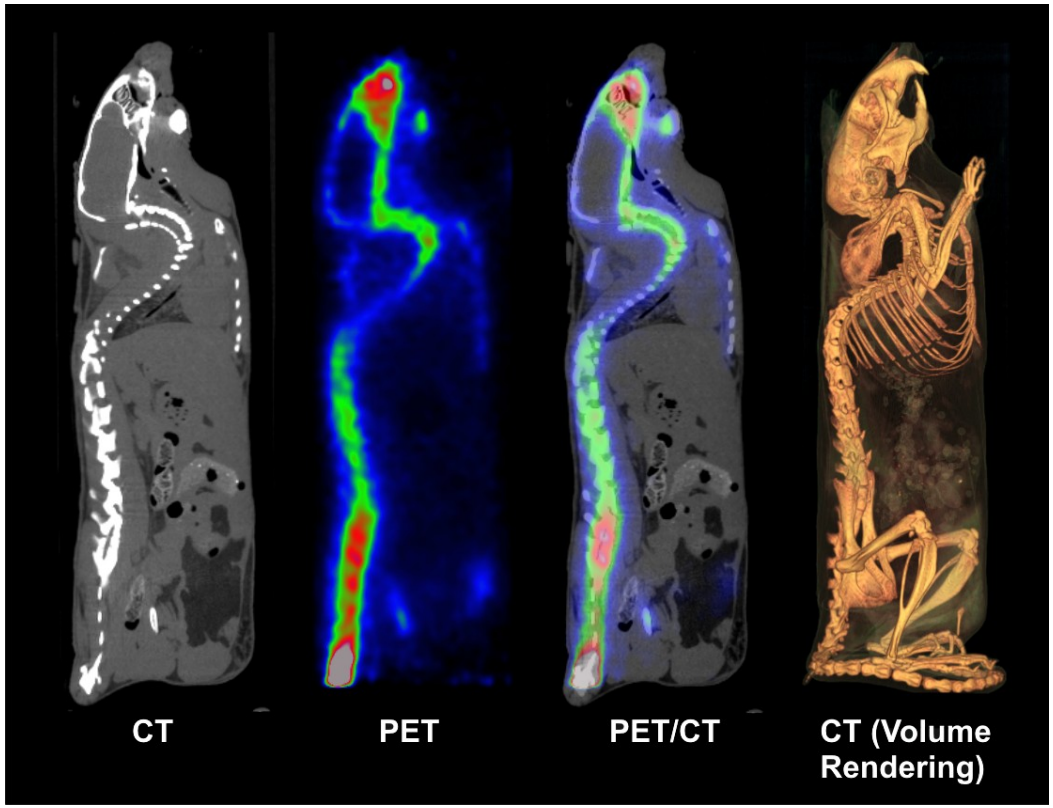

Hybrid imaging applications to a mouse

From left to right: CT image, PET image, fused image and volume rendering of the CT image

Study of neo-angiogenesis of stroke model in rats

Scope: evaluate the applicability of a PET tracer for the neoangiogenesis in a heart stroke model in rats.

Materials: Use of $\alpha_V\beta_3$ **integrine** as membrane receptors involved in neoangiogenesis. A integrine ligand marked with 68-Ga was used to visualize neoangiogenesis.
Ammonia (13-N) was used to visualize local perfusion in the heart and to evaluate the extension and location of the stroke.

Method: 2 groups were studied: (a) rats with a stroke caused by occlusion of the LAD – Left Anterior Descending coronary;
(b) sham rats (same surgery intervention without occlusion).

Heart ischemia in rat (multimodality PET-CT)

Sham-operated **LAD occluded**

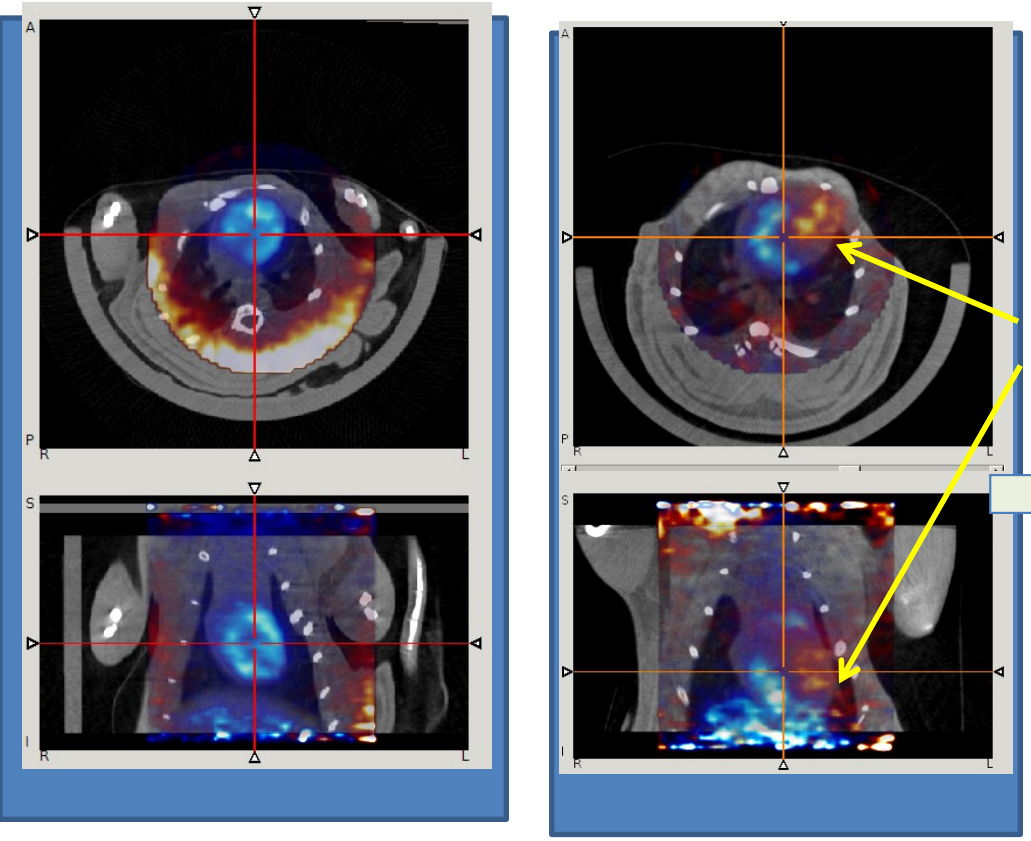

^{68}Ga-RGD ($\alpha_5\beta_3$ integrin ligand)

$^{13}NH_3$ (perfusion)

Perfusion defect/
Integrin overexpression

PET/CT imaging with $^{13}NH_3$ + ^{68}Ga with YAP-(S)PET+Xalt

(courtesy of L. Menichetti, P. A. Salvadori, IFC-CNR Pisa, and A. L'Abbate, SSSUP)
Preliminary data unpublished

Hybrid Systems II
PET/MR

MR/PET:“one-stop-shop”

New whole-body imaging procedures allow comprehensive imaging examinations

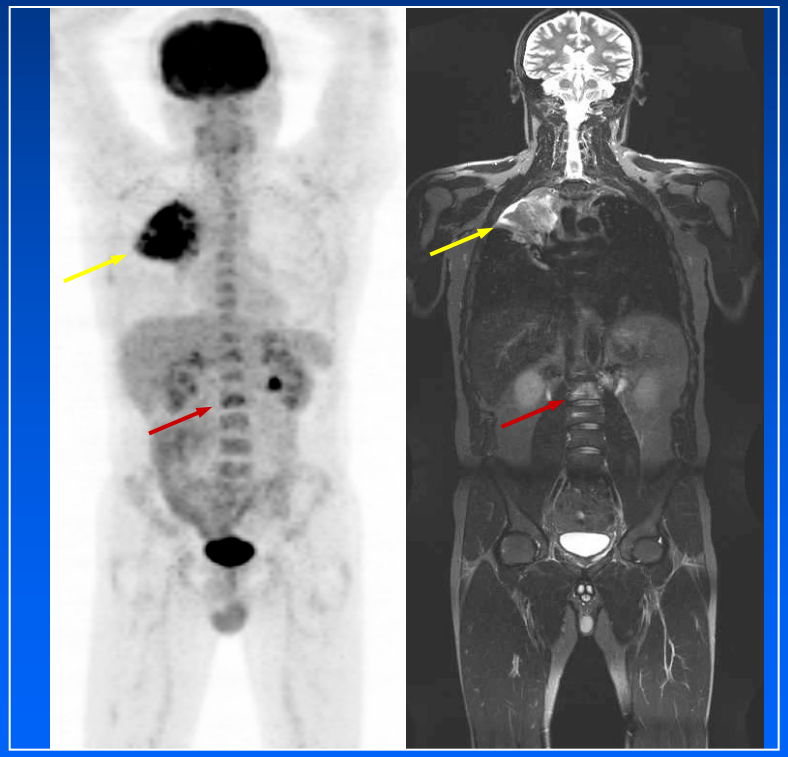

Coronal overview of 18F-FDG PET and MRI (T2- weighted Turbo-STIR)

Fused MRI/PET facilitates accurate registration of morphological and molecular aspects of diseases

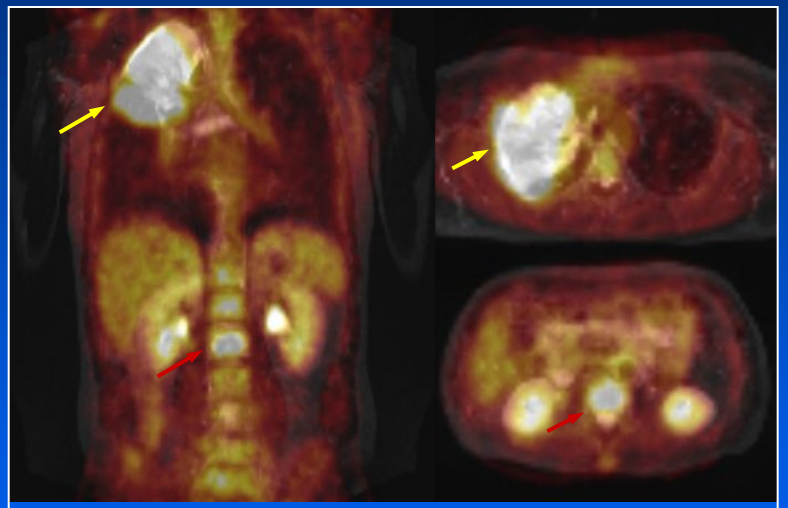

Pulmonary and osseous (arrow, red) metastatic disease of a non-small cell lung cancer (arrow, yellow)

Coronal and transversal MRI/PET fusion images

Courtesy of Dr. Gaa, TU Munich

Why PET/MR?

- Strengths
  - "Near-perfect" registration of structural and molecular imaging data
  - Anatomically-guided interpretation of PET data
  - Anatomic priors for PET reconstruction and data modeling
  - PET can be combined with other MRI techniques such as DWI, DCE MR, MRS, cell tracking and MR molecular imaging agents
- Weaknesses
  - Technically difficult and more expensive
  - Uncertainty regarding throughput, cost effectiveness and ultimate clinical role

Technical Challenges in simultaneous PET/MRI

- Interference on PET
  - Static magnetic field
  - Electromagnetic interference from RF and gradients
- Interference on MR
  - Electromagnetic radiation from PET electronics
  - Maintaining magnetic field homogeneity
  - Eddy currents
- General Challenges
  - Space
  - Environmental factors (temperature, vibration…)
  - Cost

PMT Sensitivity to Magnetic Fields

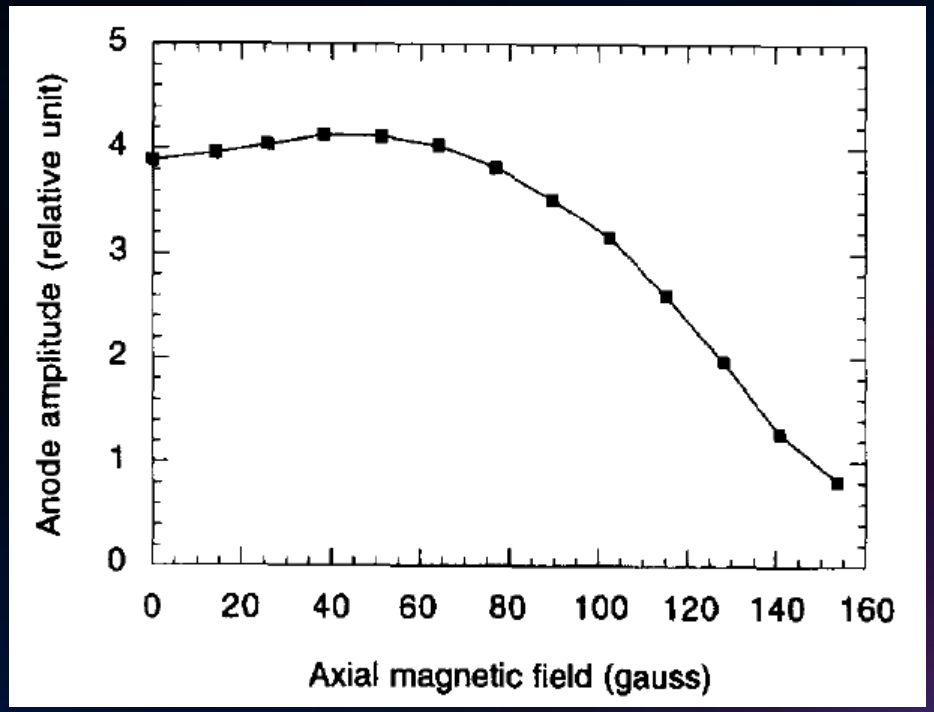

3T = 30,000 gauss; 7T = 70,000 gauss!

Integrated PET/MRI System

Concept

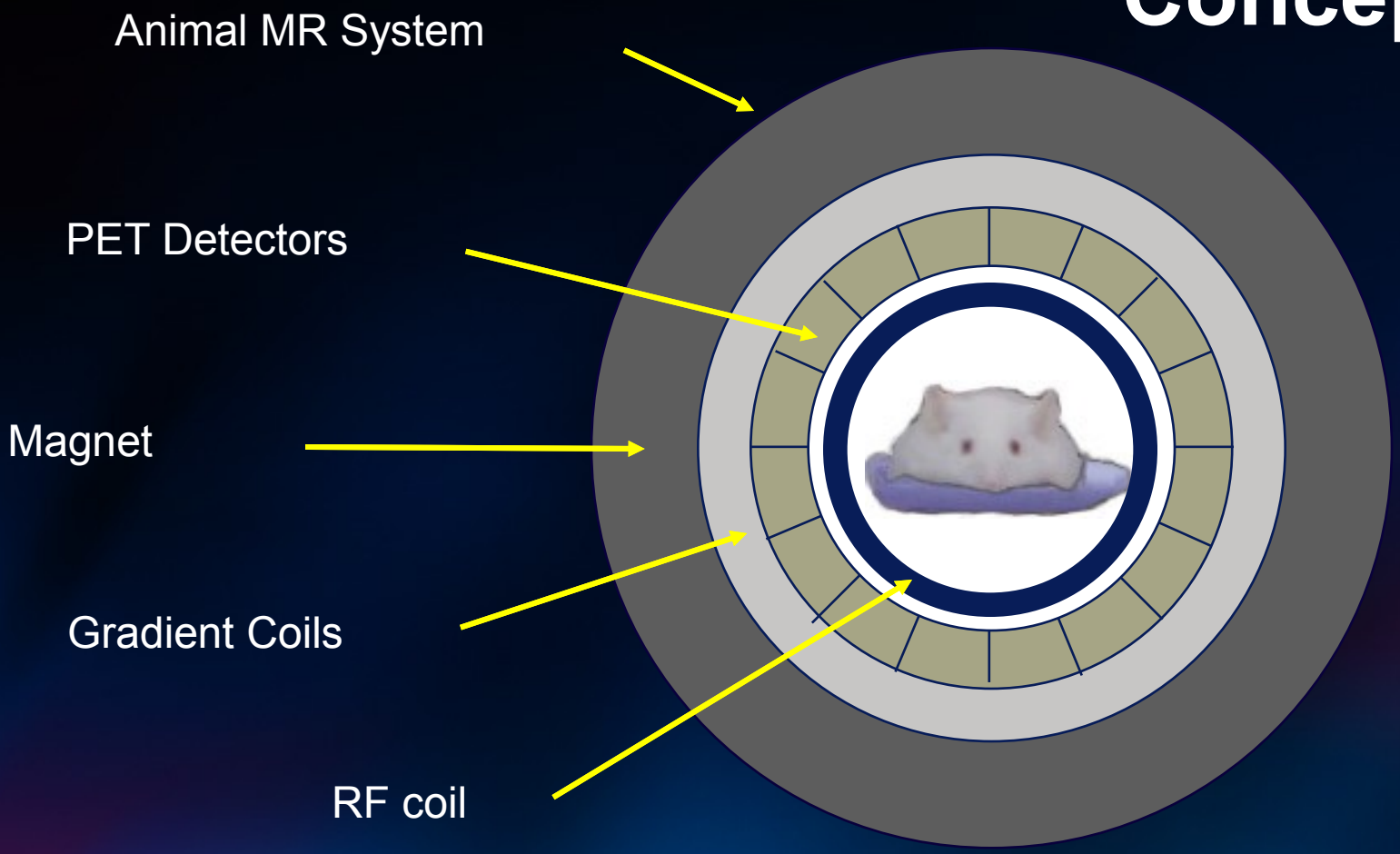

Fiber-Optic Based PET/MRI

- Challenges
  - Number of detector elements limited by volume of fiber-optics
    - Fiber-optic based PET/MRIs typically have up to a few hundred detectors
    - Modern PET scanners have >10,000 detectors!
  - Long fibers result in degraded
    - Crystal identification
    - Energy resolution
    - Timing resolution

Split Magnet PET/MRI

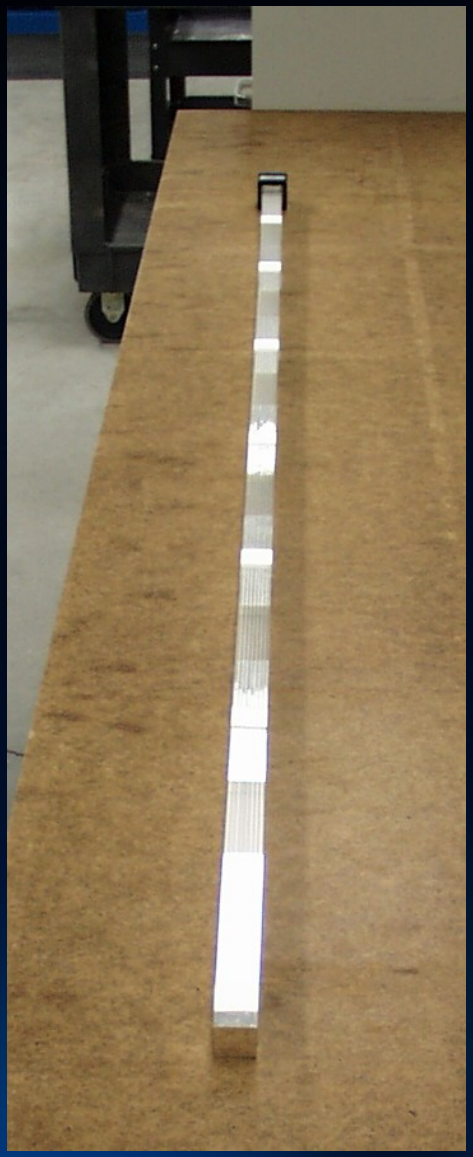

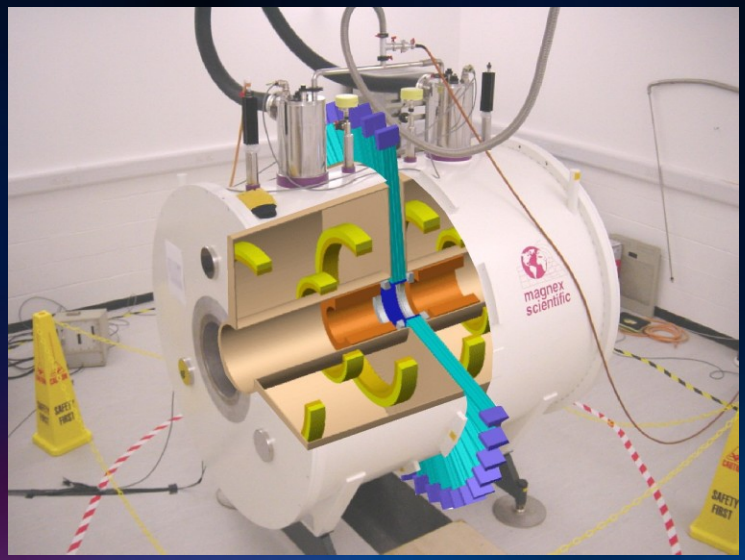

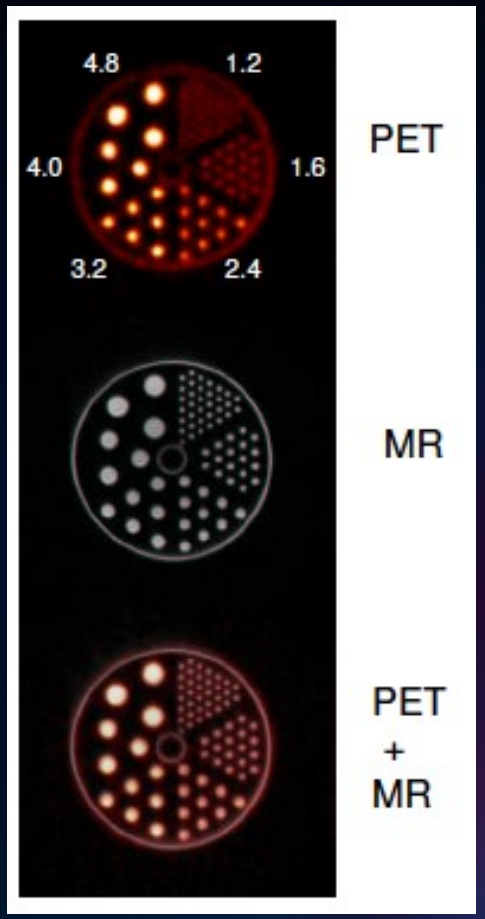

A Lucas, R. Hawkes, P Guerra, R Ansorge, R Nutt, J Clark, T Fryer, A Carpenter

UNIVERSITY OF CAMBRIDGE

SiPM-Based PET/MRI

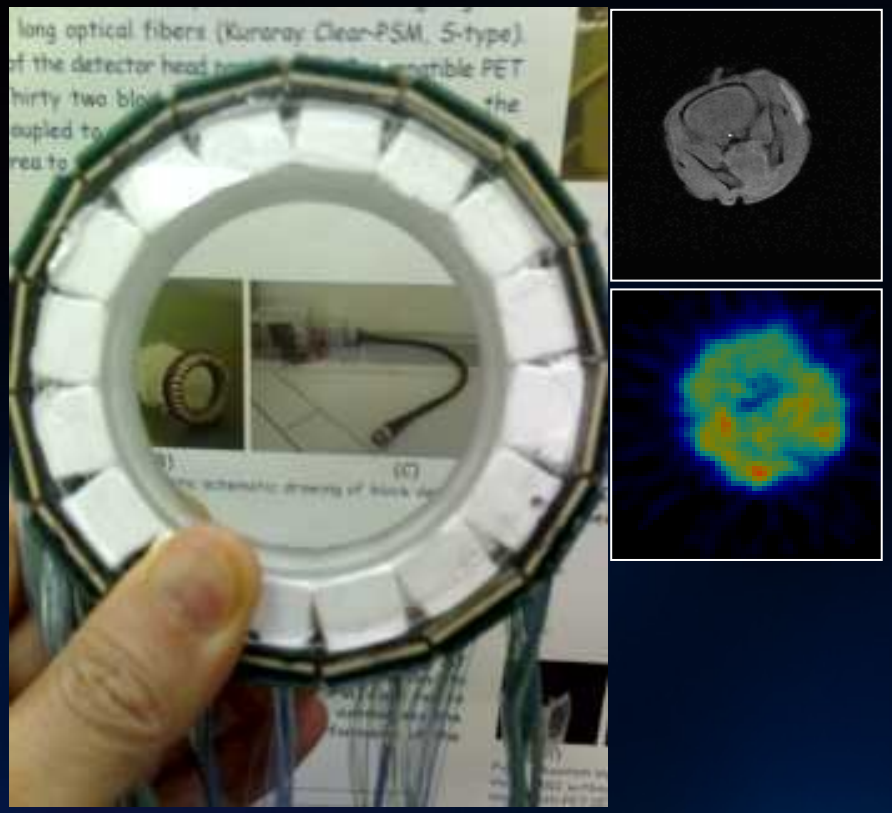

Courtesy of Seiichi Yamamoto
Kobe University

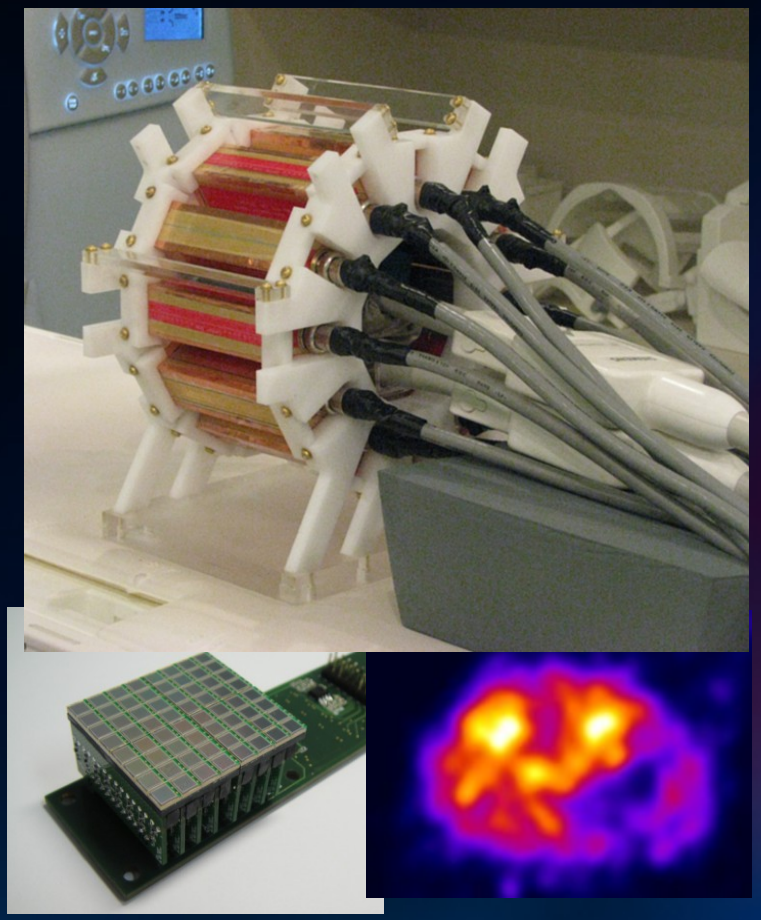

Courtesy of Jae Sung Lee,
Seoul National University

PET/MRI
endless possibilities

MRI

Structural imaging

fMRI

DCE MRI

DTI

MR Spectroscopy

paraCEST

Hyperpolarized ^{13}C

…

PET

Metabolic imaging

Blood flow

Receptor ligands

Hypoxia

Proliferation

Amyloid imaging

Cell trafficking

…

PET/MRI

ULTRA HIGH FIELD MR

$ for a better spatial resolution

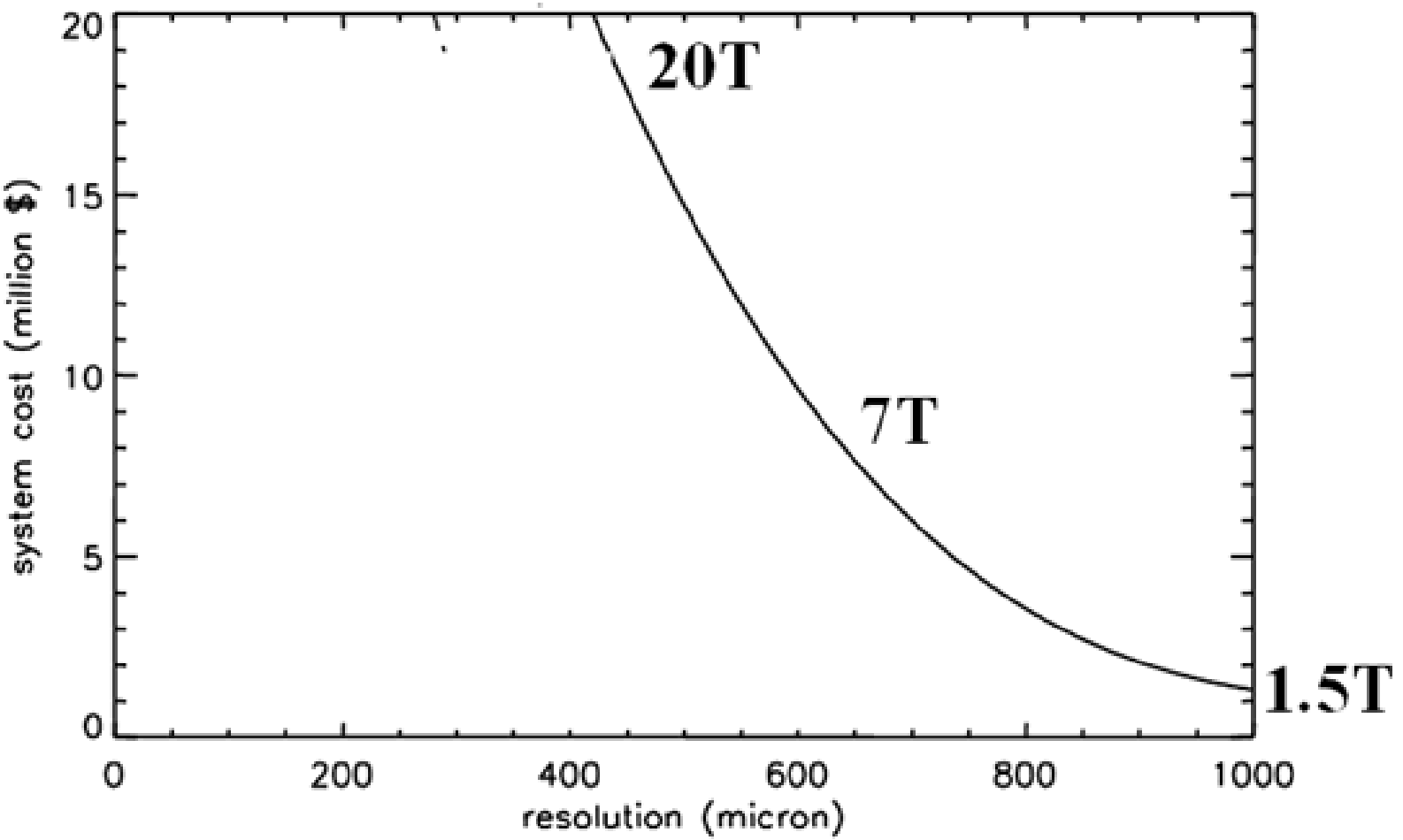

The evolution of MR images

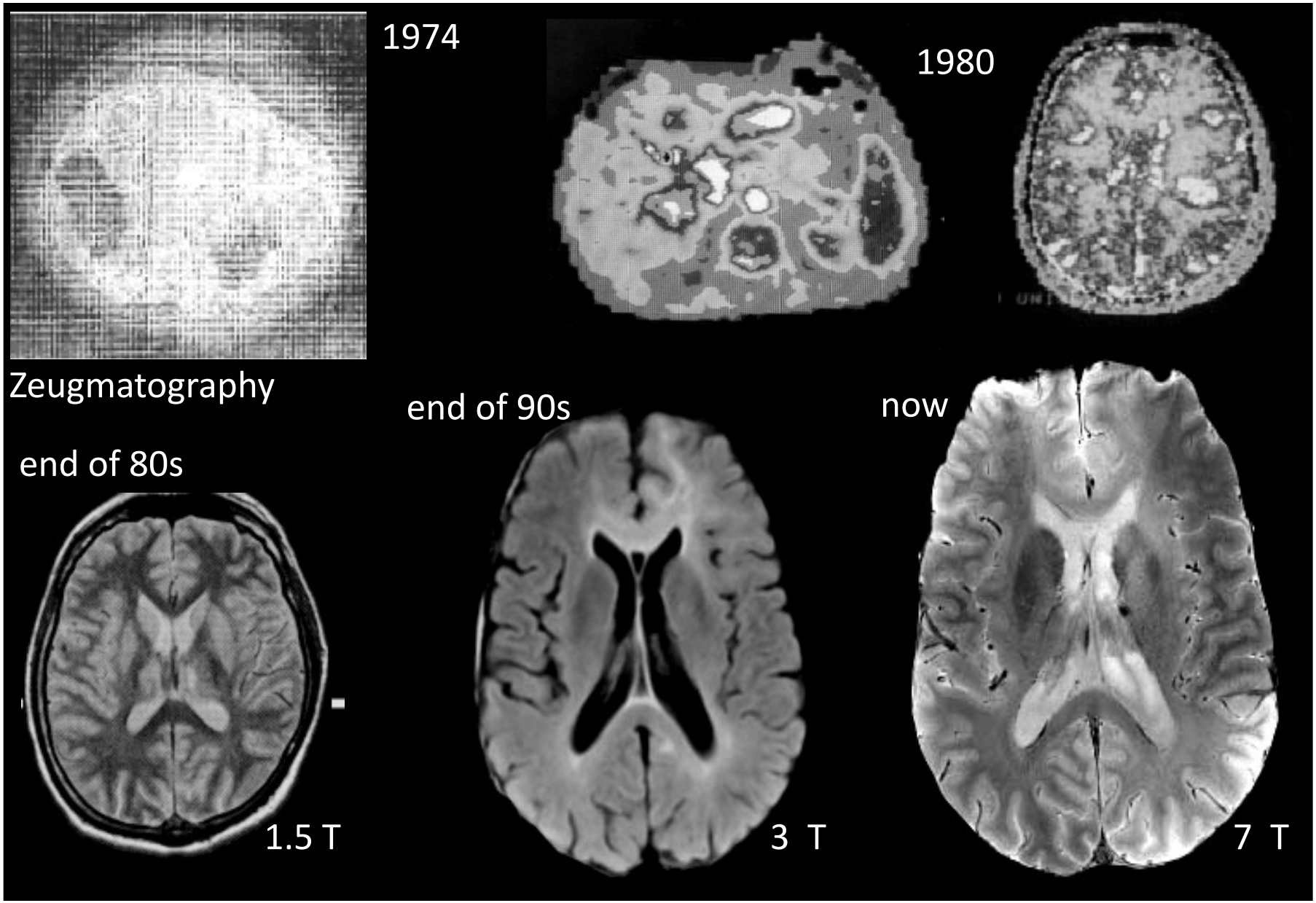

THE PISA *IMAGO7* RESEARCH FOUNDATION

The Stella Maris Scientific Institute, Pisa
IRCCS for Developmental Neurology,
Psychiatry and Rehabilitation

GE imagination at work

GE SIGNA 7T

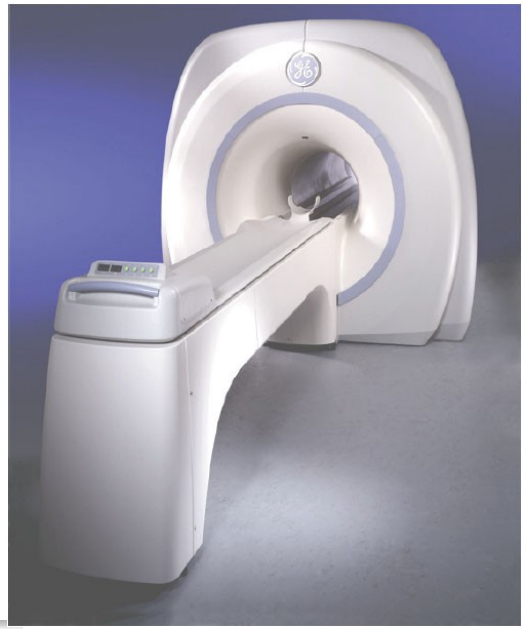

The University of Pisa
Department of Physics
Department of Chemistry
Department of Neuroscience
Laboratory of Clinical Biochemistry and Molecular Biology

The Pisa University General Hospital
Department of Radiology

The MEDEA Scientific Institute, Bosisio Parini (Lecco)
IRCCS for Developmental Neurology,
Psychiatry and Rehabilitation

EUGENIO MEDEA

The CARIPI Foundation (Pisa)

CariPisa la FONDAZIONE

Status of the IMAGO7 center

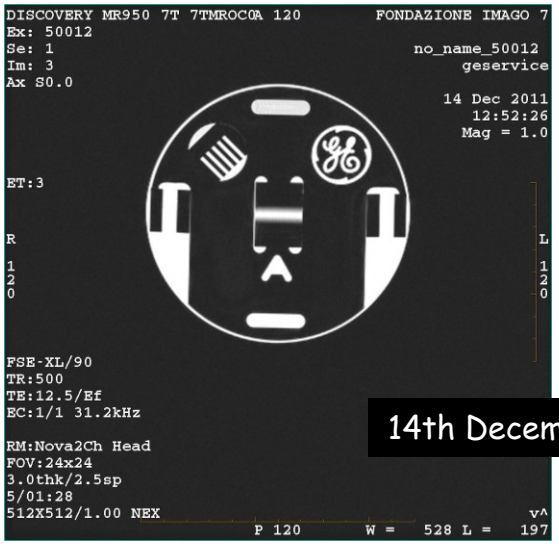

14th December 2011

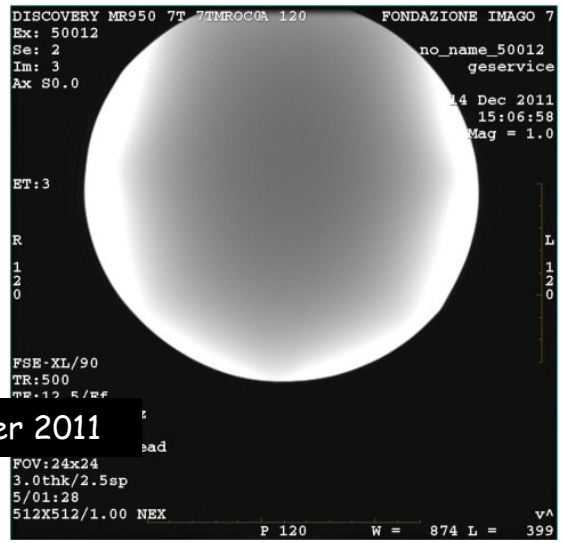

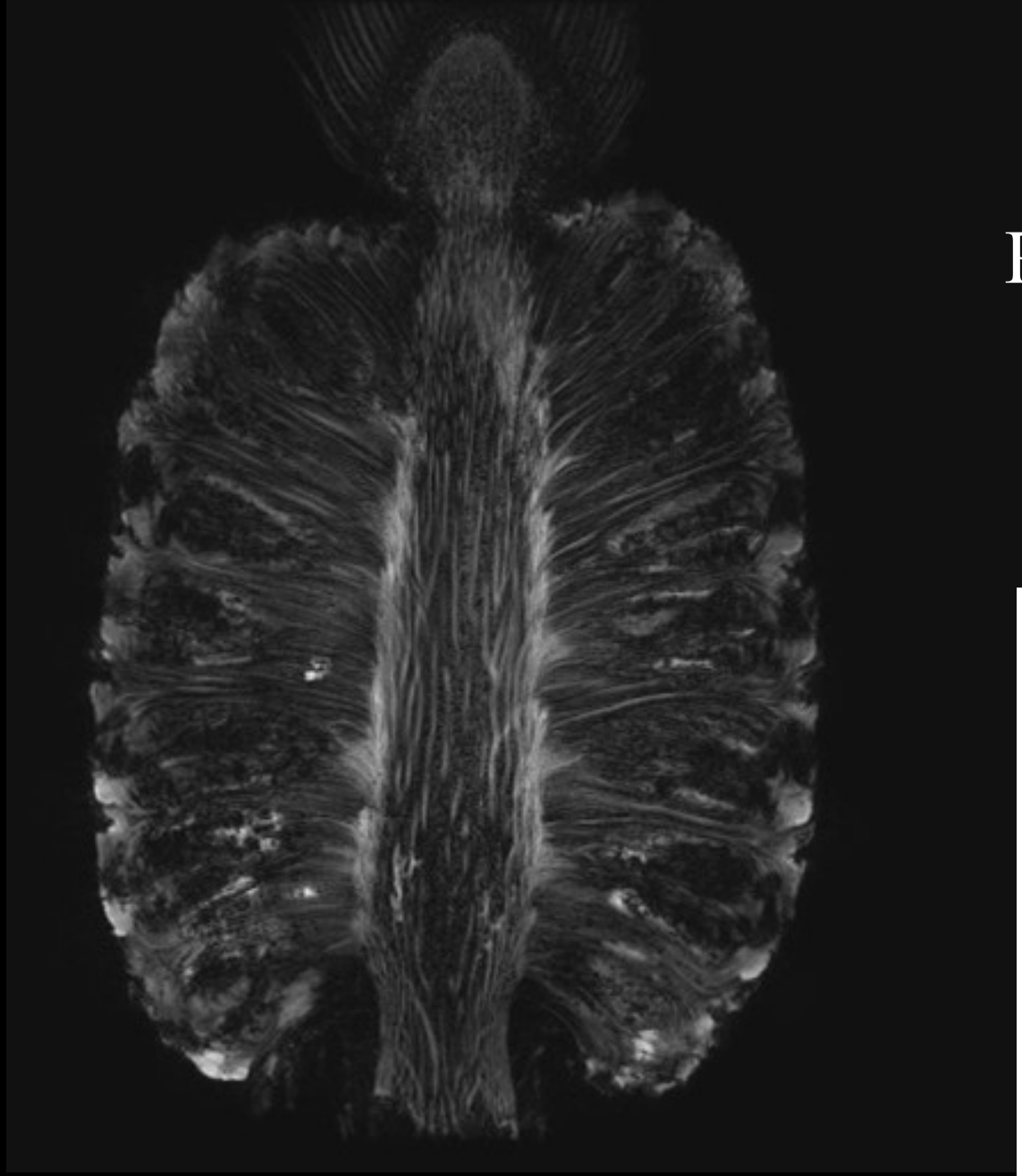

Pisa, January 2012

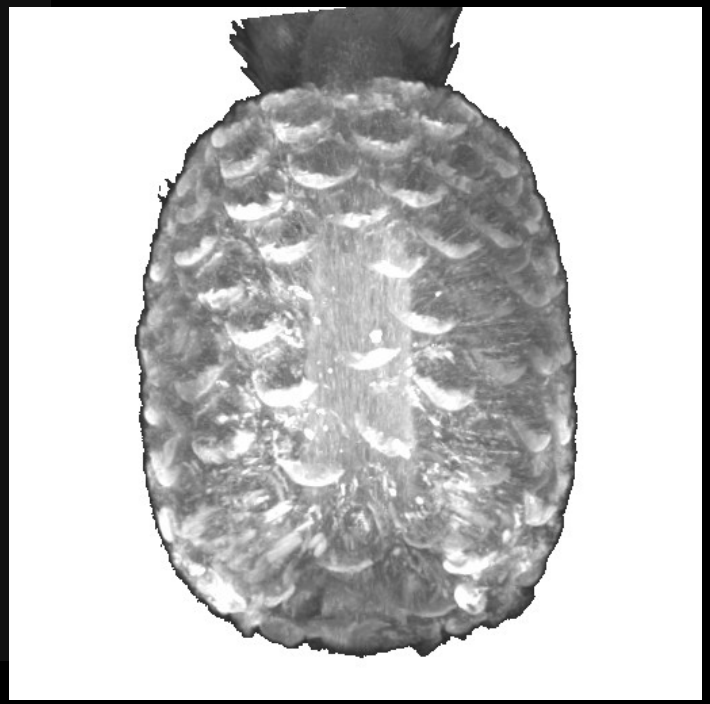

An application in RADIATION ONCOLOGY

Rationale for Hadron-Therapy

- Starting point of proton-therapy

R.R Wilson, "Radiological Use of Fast Protons" Radiology, 47, pp. 487- 491, 1946.

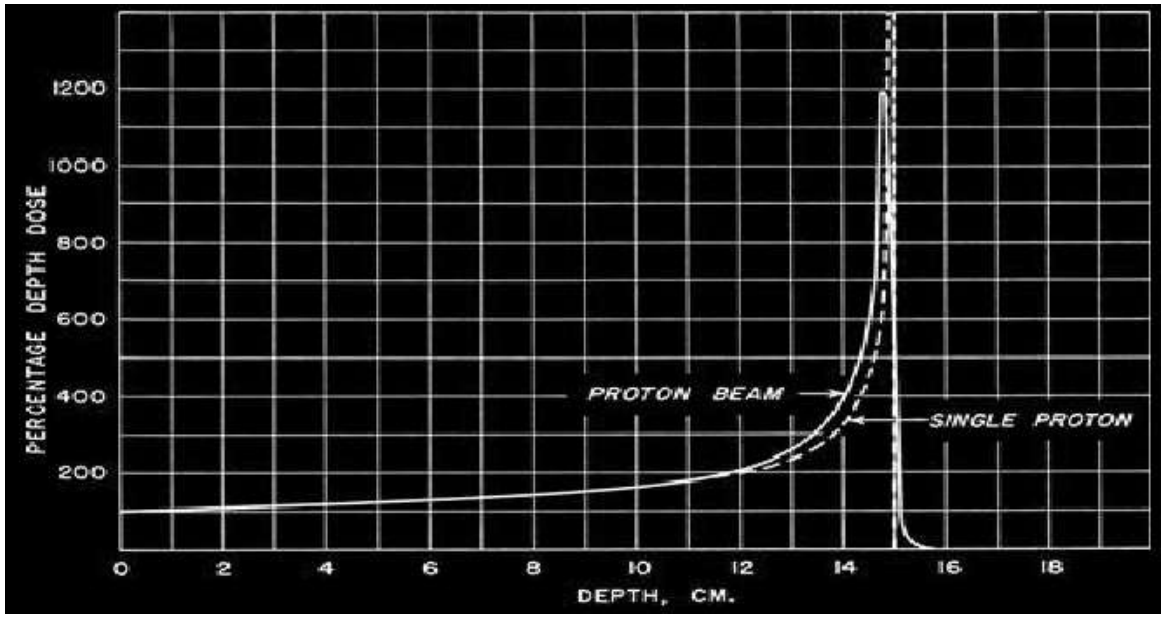

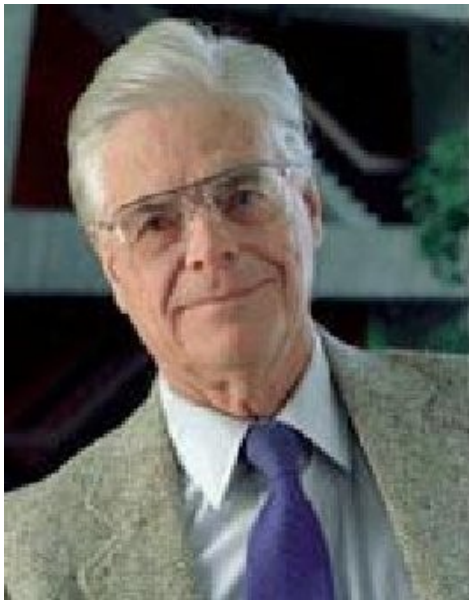

1. *Protons can be used clinically due to the availability of accelerators*
2. *Maximum radiation doses can be placed into the tumor*
3. *Proton therapy spares normal tissues*
4. *Modulator wheels introduce energy modulation to reach Spread-Out Bragg Peak*

Advantages of Hadrontherapy

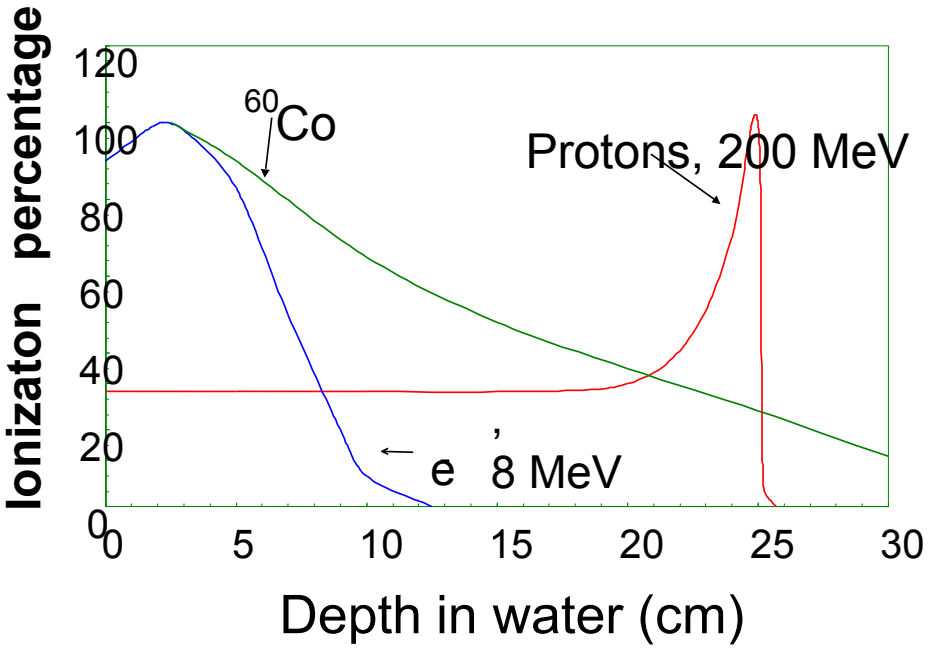

- **More dose delivered in depth**
- **Better dose conformation for the same total dose**

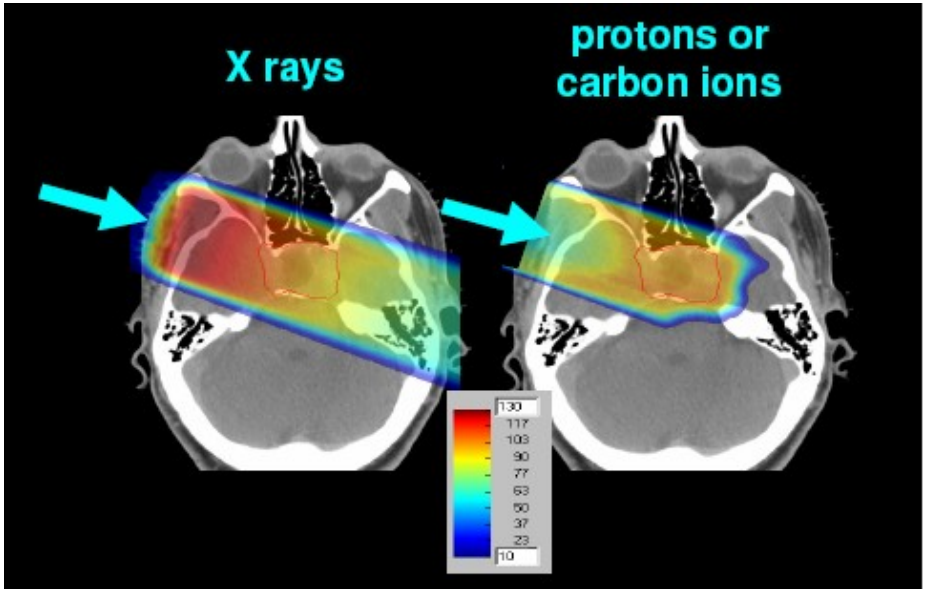

Rationale for Hadron-Therapy

Why Hadron-Therapy?

- Sharp dose fall-off after the Brag Peak
- Higher Relative Biological Effectiveness
- Highly conformal
- More focused on tumor
- Max dose at last mm particle's range (BP)

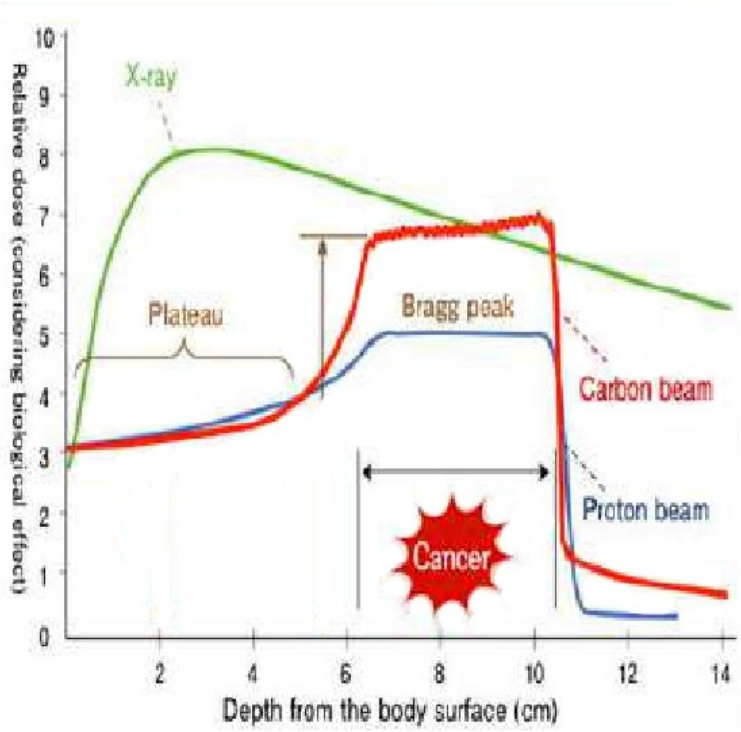

◆ Proper spatial superimposition of several Bragg-peaks of different depths and amplitudes, enables optimal conformation of the delivered dose to the tumor volume.

◆ The depth of the Bragg Peak depends on the initial energy of the ions, while its width on the straggling and on the energy spread of the beam has to be small.

Hadrotherapy in Italy: **Catana** at the "Laboratori Nazionali del Sud", INFN Catania

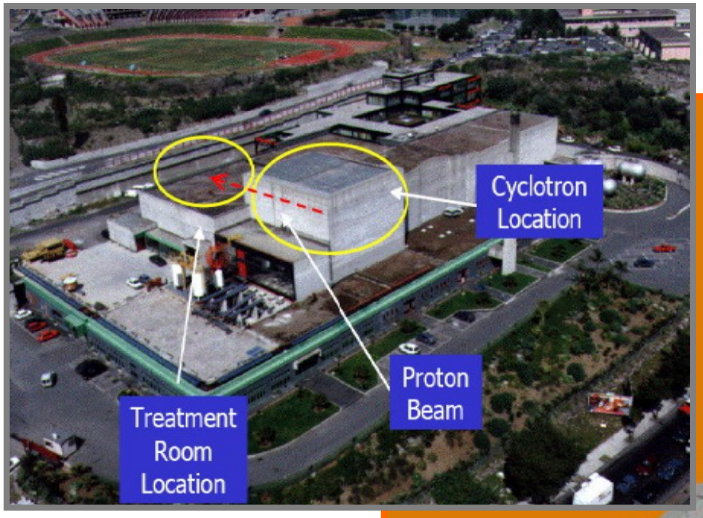

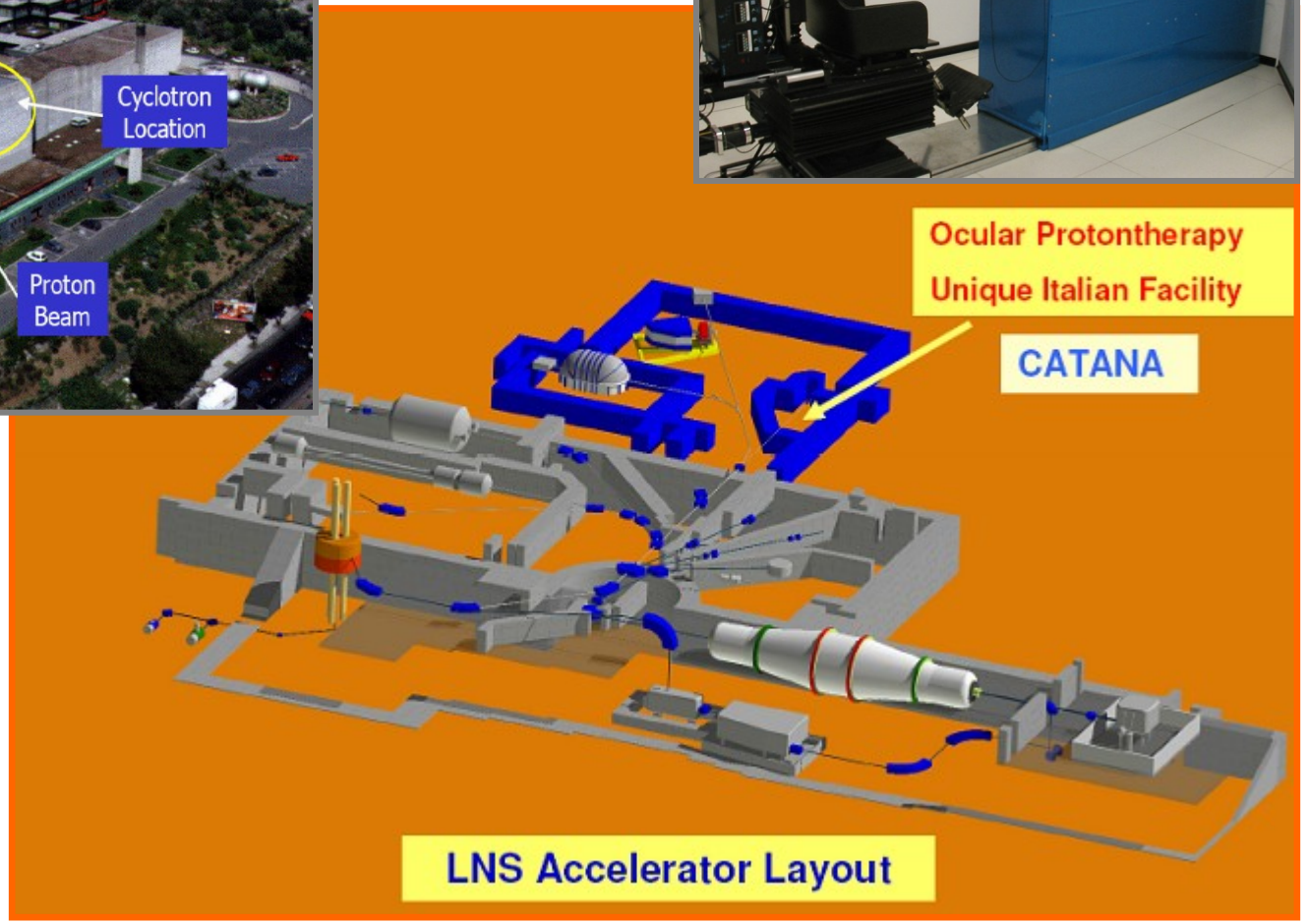

New Hadrontherapy Center in Italy (Pavia at the S.Matteo)

CNAO - Centro Nazionale di Adroterapia Oncologica

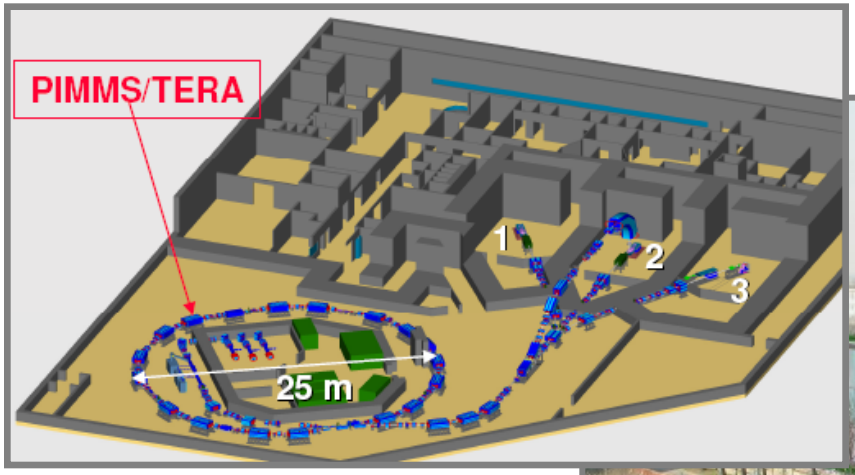

Treatments both with protons and carbon ions.

Three treatment rooms; in one room a vertical beam will be also available.

In-beam PET monitoring

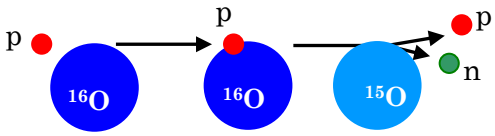

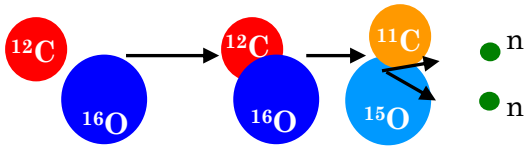

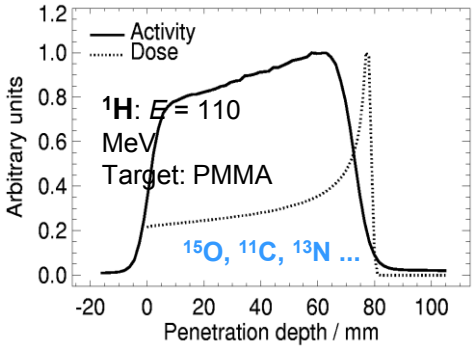

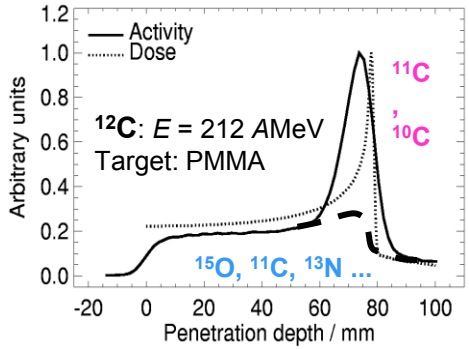

In-beam/in-room dedicated instruments are necessary to:
- Avoid patient re-positioning
- Avoid data loss of very short living isotopes

A possible method for the control of the geometrical accuracy of the treatment (TPS) is PET imaging

- **Nuclear inelastic reactions between the hadron beam and nuclei in tissue**
- **Small amounts of β^+ emitting isotopes are produced with short half-lives like**
  - **^{11}C (20.3 min),**
  - **^{13}N (9.97 min),**
  - **^{15}0 (2.03 min).**

Rationale for “On-Line”PET

- Dose Activity: Standard Approach

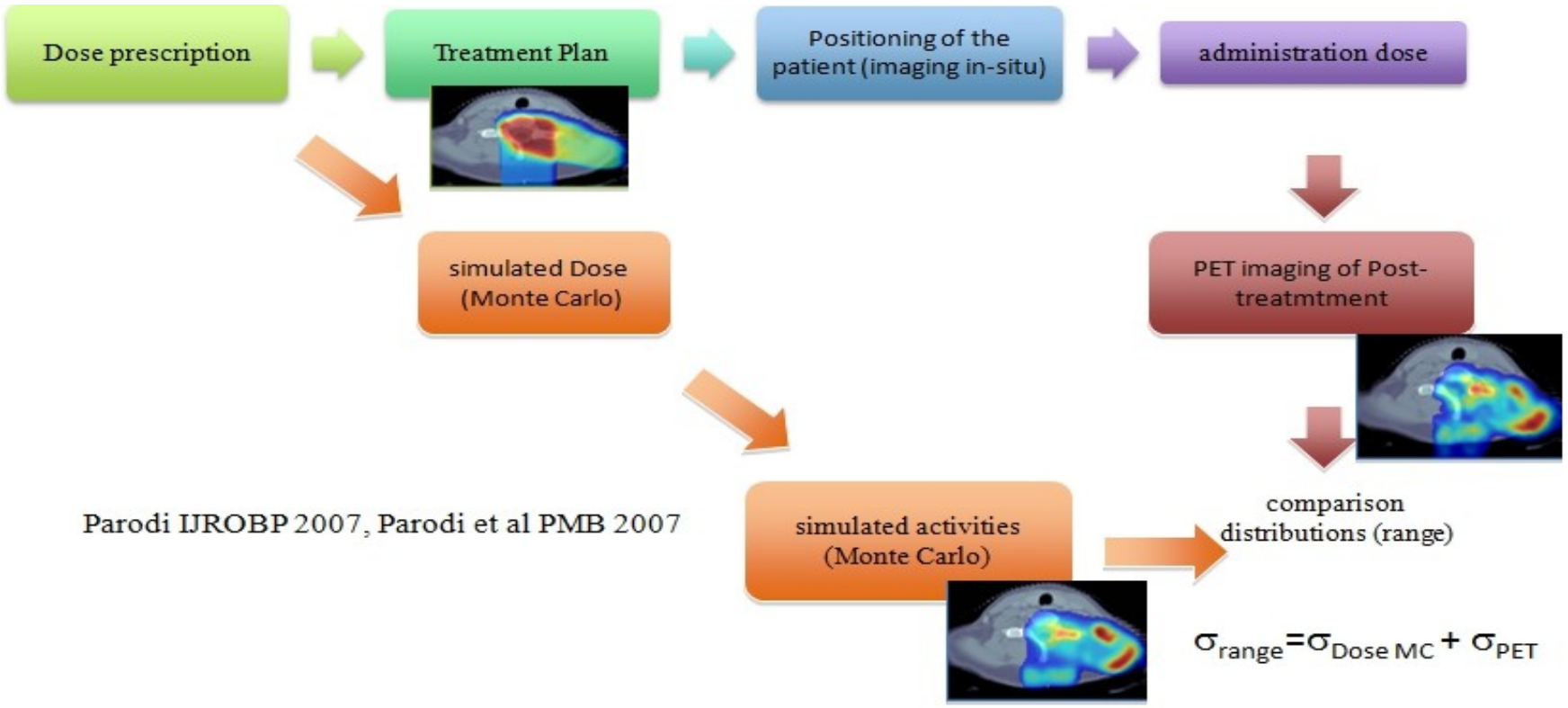

- Comparison between simulated activity and measured activity with PET

Rationale for "On-Line" PET

- Dose Activity: The "Filtering"

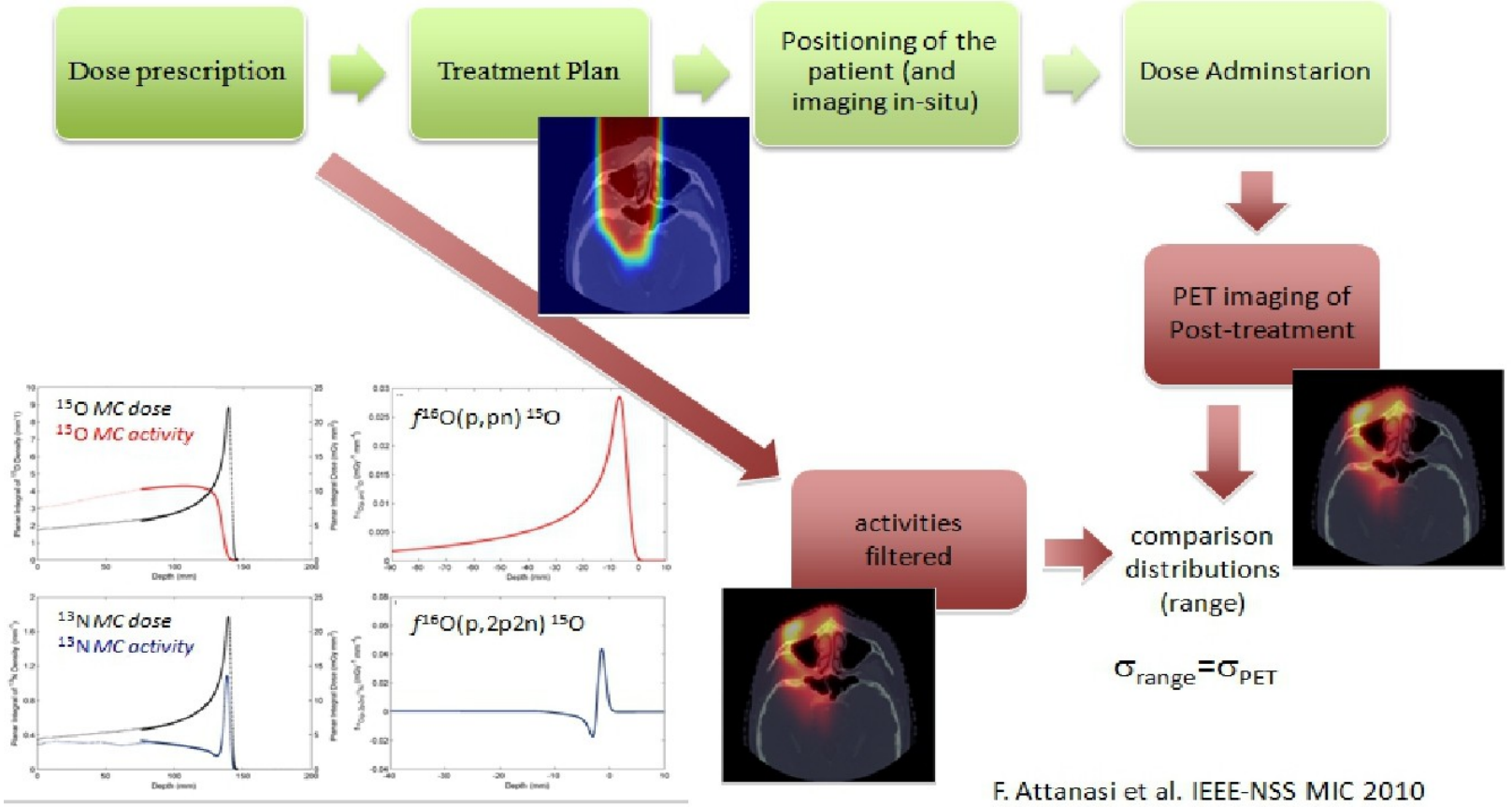

- From the planned dose, the activity profile is obtained by using filter approach

Rationale for “On-Line”PET

- Next step: The Reverse Filter

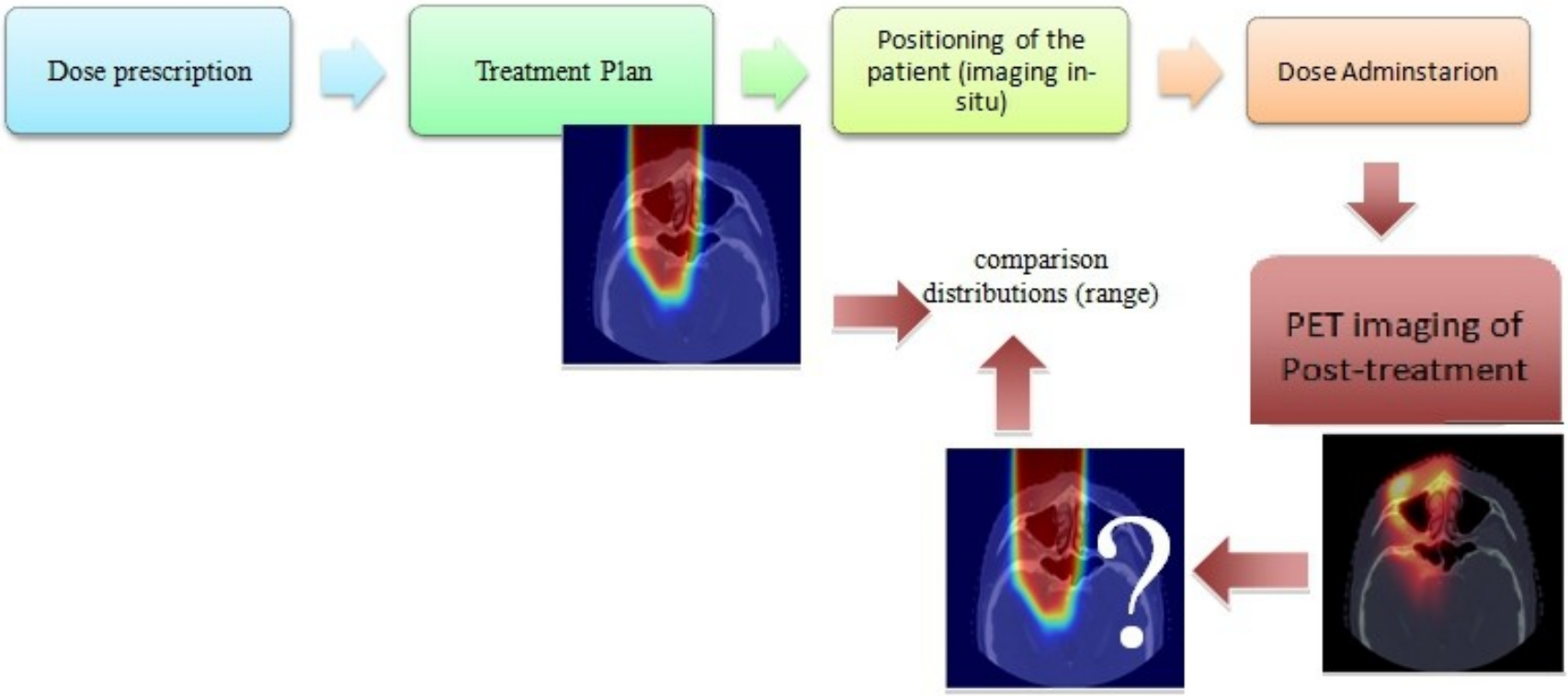

- The delivered dose is measured from the measured activity of PET by using the inverse filtering
- The planned dose can be compared with the measured dose

The System Description

- The configuration

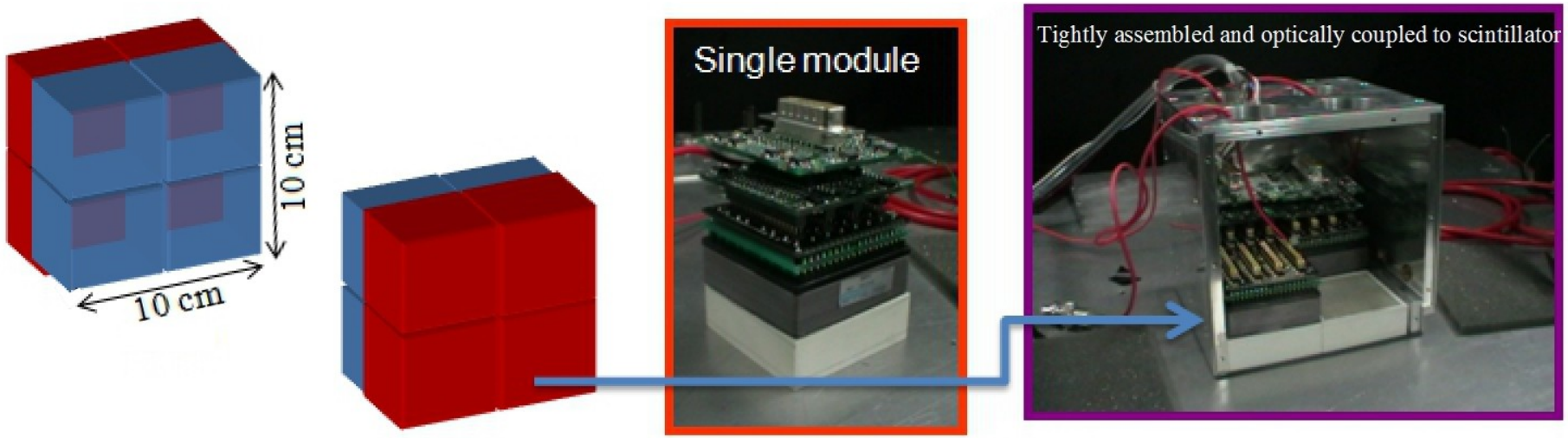

- **Two planar head of 10.4x 10.4 cm^2 per each head**
- **The total active area of each crystal is 4.6 4x 4.6 cm^2**
- **Each scintillator is a LYSO matrix of 23x23 pixels (1.6x1.6x19 mm^2) with a pitch of 2mm**

DoPET – TPS (INFN)

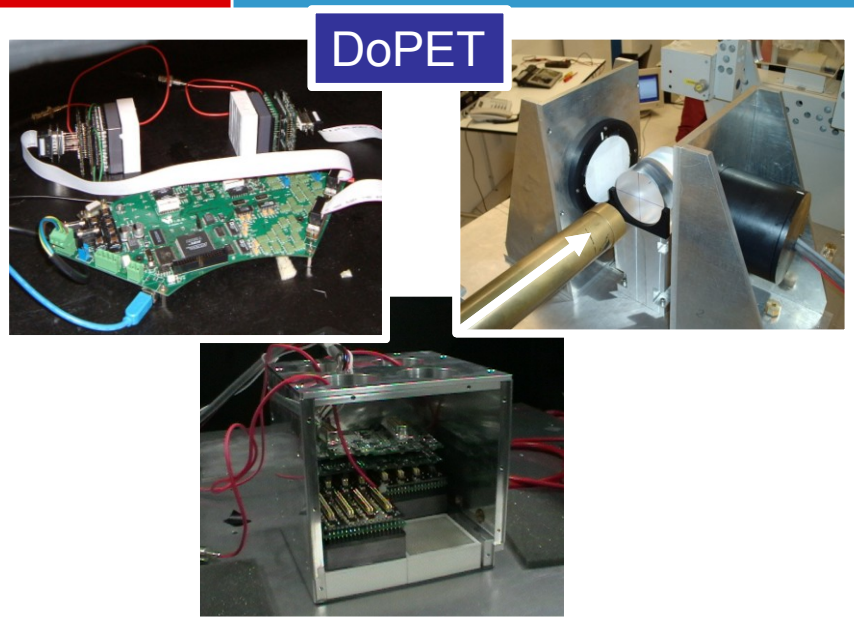

A dedicated PET system for in-room (in-beam) dose monitoring in Hadrontherapy

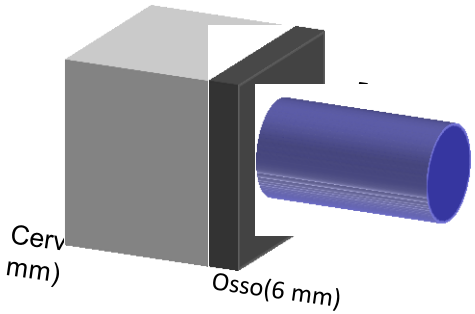

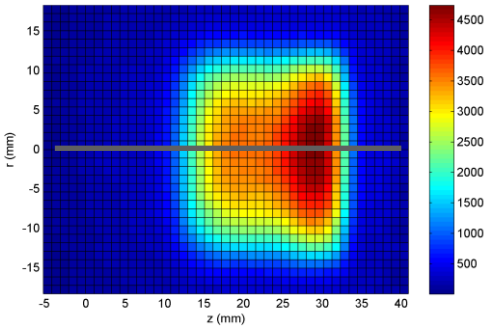

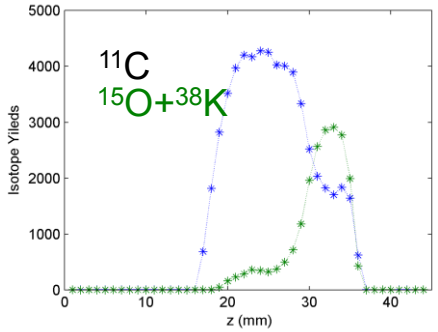

PET image of the activity distribution produced in tissue equivalent phantoms irradiated with protons. The contribution of different isotopes is separated with decay time analysis.

A FINAL DIGRESSION

RESEARCH and Profession
in
MEDICAL PHYSICS
(a personal view)

MEDICAL PHYSICIST

*"**Medical physicists** are professionals with education and specialist training in the concepts and techniques of applying physics in medicine. Medical Physicists work in:*

- *clinical*
- *academic*
- *research institutions.*

***Medical physicists working in the clinical environment** are health professionals, with education and specialist training in the concepts and techniques of applying physics in medicine, competent to practice independently in one or more of the sub-fields (specialities) of medical physics."*

Qualification Framework for the Medical Physics Expert (MPE) in Europe

MPE: "An individual having the knowledge, training and experience to act or give advice on matters relating to radiation physics applied to medical exposure, whose competence to act is recognized by the Competent Authorities" (Recast BSS)

The Qualifications Framework is based on the European Qualifications Framework (EQF). In the EQF learning outcomes are defined in terms of Knowledge, Skills, Competences (KSC) (European Parliament and Council 2008/C 111/01)

EDUCATION

EQF Level 6
(e.g., Bachelor with 180 - 240 ECTS)
(i)

Physics
or
equivalent
(ii)

EQF Level 7
(e.g., Master with 90 - 120 ECTS)
(iii)

Medical Physics
or
equivalent.
(iv)

CLINICAL TRAINING

To Medical Physicist
(v)

Accredited residency based training in the specific area/s of Medical Physics* for which the candidate seeks recognition as Medical Physicist. The duration of this training is *two* full-time year equivalents for the *first* area of Medical Physics, plus *one* further full-time year equivalent for *each* additional area.
(vi)

EXPERIENCE and CPD

To EQF Level 8
(vii)

Advanced experience and CPD in the specific area/s of Medical Physics for which the candidate seeks recognition as MPE. The duration would be a *further additional two years beyond* the level of Medical Physicist for the *first* area of Medical Physics, plus *one* further full-time year equivalent for *each* additional area.
(viii)

RECOGNITION

By Competent Authorities as MPE in specific area/s of Medical Physics
(ix)

RE-CERTIFICATION

5 year CPD cycle
(x)

* Diagnostic and Interventional Radiology, Nuclear Medicine, Radiation Oncology

CONCLUSIONS

from: CERN Academic Training Program *"Lecture Series - Detectors application in Medicine and Biology"*, Alberto Del Guerra, January 9-13, 1995

Problems solved for HEP experiments

1. μ-strip silicon detector for charged particle tracking
2. Typical dimension: 4x (5x5 cm^2); thickness $\leq$ 500 μm
3. Electronics for m.i.p. (in 300 μm $\approx$ 70 keV energy loss)
   - low noise: 500-1000 e^-
   - reasonably fast: 100-1000 ns
   - integration on VLSI
4. External Trigger
5. DAQ for collider
   - low multiplicity
   - fast acquisition
   - sparse readout
6. **Number of channels: 10^5-10^7**
7. Event size (raw data): 10^6 bytes (level 1 trigger)
8. **Number of sellable apparatus: 1 (maybe two!!)**

But the apparatus is made of thousands of modules ➔ Hence…Redundancy!

from: CERN Academic Training Program *"Lecture Series - Detectors application in Medicine and Biology"*, Alberto Del Guerra, January 9-13, 1995

Problems to be tackled for Imaging with X-rays (10-100 keV): Digital Radiology

1. μ-strip silicon detector for X-rays
2. Required dimension: 20x20 cm^2; thickness (300 μm – 3 mm)
3. Electronics for X-rays (down to 10 keV)
   - low noise: 200 e-
   - fast: 10-100 ns
   - integration on VLSI
4. Self-Triggering
5. DAQ for Digital Radiology
   - $5x10^4$ Hz/mm^2 (on a 20x20 cm^2 $2x10^9$Hz)
   - 1 s acquisition time (duty cycle 100%)
6. **Number of channels: 10^3-10^4**
7. Event size: 1 bit - 10 bytes
8. **Number of sellable apparatus: 10^3-10^6**

Take Home Message

- *Wrong approach: Detector driven*

  "I have the best detector for… what??"

- *Right approach: Experiment driven*

  "I have this biological, medical, clinical experiment to make with these requirements: ➔ which is the best detector to be used, built or developed ?"

[Courtesy of Hedvig Hricak, Memorial Sloan-Kettering Cancer Center, ECR - 2009]

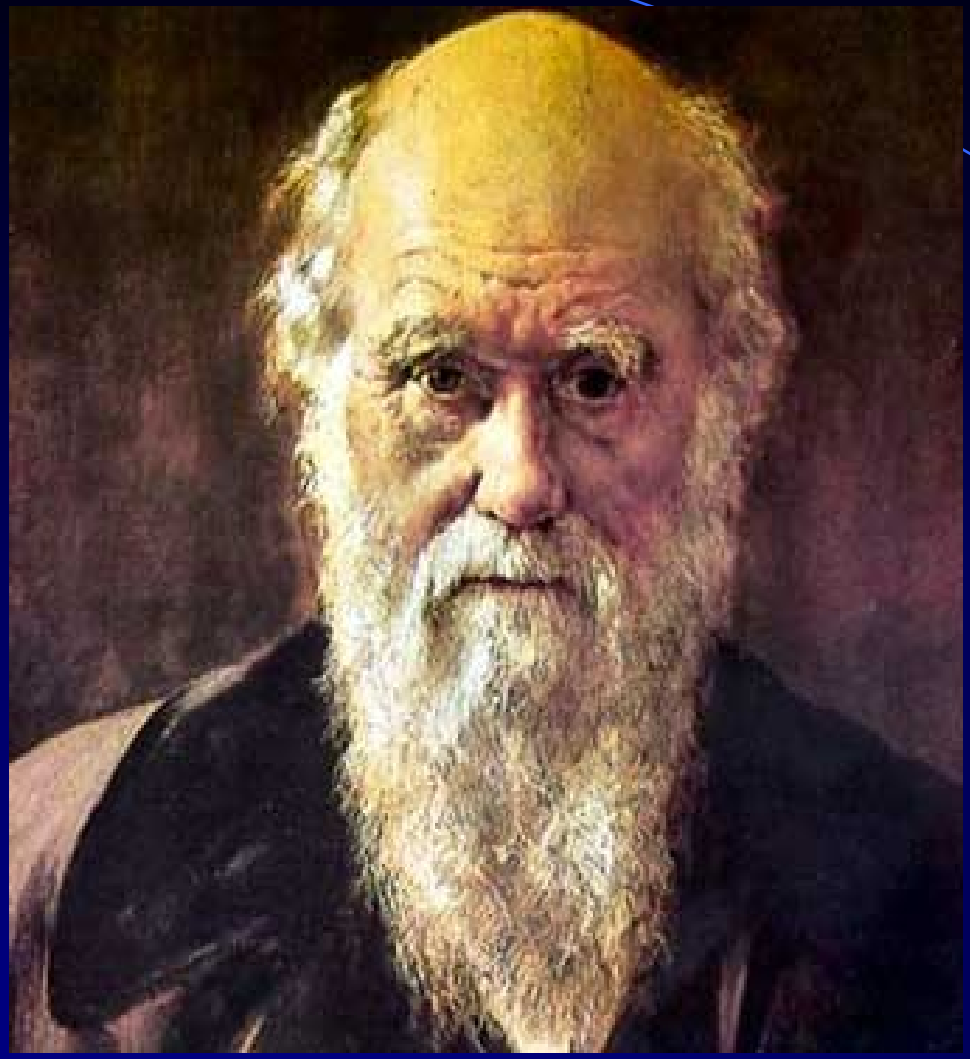

Charles Darwin
Feb 12, 1809 – April 19, 1882

Charles Darwin
The origin of Species
November 1859

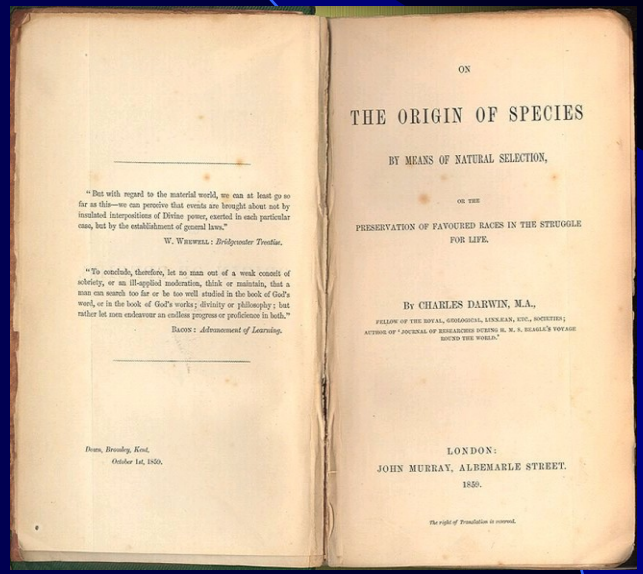

"But with regard to the material world, we can at least go so far as this—we can perceive that events are brought about not by insulated interpositions of Divine power, exerted in each particular case, but by the establishment of general laws."

W. WHEWELL: *Bridgewater Treatise.*

"To conclude, therefore, let no man out of a weak conceit of sobriety, or an ill-applied moderation, think or maintain, that a man can search too far or be too well studied in the book of God's word, or in the book of God's works; divinity or philosophy; but rather let men endeavour an endless progress or proficience in both."

BACON: *Advancement of Learning.*

Down, Bromley, Kent,
October 1st, 1859.

ON

THE ORIGIN OF SPECIES

BY MEANS OF NATURAL SELECTION,

OR THE

PRESERVATION OF FAVOURED RACES IN THE STRUGGLE FOR LIFE.

By CHARLES DARWIN, M.A.,

FELLOW OF THE ROYAL, GEOLOGICAL, LINNEAN, ETC., SOCIETIES;
AUTHOR OF 'JOURNAL OF RESEARCHES DURING H. M. S. BEAGLE'S VOYAGE ROUND THE WORLD.'

LONDON:
JOHN MURRAY, ALBEMARLE STREET.
1859.

The right of Translation is reserved.

"It is not the strongest of the species that survives,
nor the most intelligent that survives.
It is the one that is the most adaptable to change."

ANATOMY LECTURE ~ 2010 – MOLECULAR

[Courtesy of Hedvig Hricak, Memorial Sloan-Kettering Cancer Center, ECR-2009]

University of Pisa -FIIG Group

FIIG Research Collaborations

Center of Excellence AmbiSEN,University of Pisa	Molecular Imaging
Istituto di Fisiologia Clinica CNR – Pisa	Molecular Imaging
Dipartimento di Medicina Nucleare,University of Pisa	Molecular Imaging
Network of Excellence EMIL **(FP6)**	Molecular Imaging
INFN – LNS Catania	Hadrontherapy
University Heidelberg / GSI (D)	Hadronterapy
Project ENVISION **(FP7)**	Hadrontherapy
MGH Boston (US)	Hadronterapy
FBK-IRST Trento	PET
INFN Bari/Bologna/Perugia/Trento	PET
University of Cambridge (UK)	PET-MRI
University of Washington (US)	PET-MRI
Project SENTINEL **(FP6)**	Radioprotection
Project HADRON PHYSICS2 – 3 **(FP7)**	Radiation detector
IMAGO7 Foundation	High Field fMRI

THANK YOU !